1-1-2014

A Mobile Self-Leveling Landing Platform for Small-Scale UAVs

Stephen Austin Conyers
University of Denver

A Mobile Self-Leveling Landing Platform for Small-Scale UAVs

_____

A Thesis

Presented to

The Faculty of the Daniel Felix Ritchie School of Engineering and Computer Science

University of Denver

_____

In Partial Fulfillment

Of the Requirements for the Degree

Master of Science

_____

by

Stephen A. Conyers

June 2014

Advisor: Dr. Matthew J. Rutherford

Author: Stephen A. Conyers
Title: A Mobile Self-Leveling Landing Platform for Small-Scale UAVs
Advisor: Dr. Matthew J. Rutherford
Degree Date: June 2014

ABSTRACT

This thesis presents a semi-autonomous mobile self-leveling landing platform designed to launch, recover and re-launch VTOL UAVs without the need for human intervention. The landing platform is rugged, lightweight and inexpensive, making it ideal for civilian applications that require a base station from which a rotorcraft UAV can be launched and recovered on terrain that is normally unsuitable for UAV operations. This landing platform is capable of self-leveling on rough terrain and inclined slopes, and can autonomously operate in remote locations for extended periods of time using large onboard lithium batteries and wireless communication. This thesis discusses the unique design aspects of this landing platform that set it apart from similar systems, describes the prototype vehicle, and shows experimental results to demonstrate the system is fully functional and meets all the primary design requirements.

This work was partially supported by NSF CNS-1229236 Grant

TABLE OF CONTENTS

LIST OF FIGURES

CHAPTER 1: INTRODUCTION

Background and Motivation

The ever-increasing popularity of autonomous Unmanned Aerial Vehicles (UAVs) for both military and civilian applications has created a need for increased autonomy in the deployment of UAVs in the field. Recent years have seen a significant increase in the capabilities of small (< 150 kg) Vertical Take-Off and Landing (VTOL) UAVs. At the same time, these vehicles have become more accessible and less expensive. Despite the rapid growth, there have been few solutions offered to address the problem of launching and recovering UAVs without human intervention. One of the difficulties associated with VTOL aircraft is that they cannot land safely on slopped or uneven terrain. This is primarily due to the physics of rotorcraft UAVs in which the thrust force is always perpendicular to the landing gear; if the vehicle is oriented to match an uneven landing surface, the vehicle may not be able to maintain flight. Additionally, when the landing surface is uneven, there is a higher chance of touching the ground with one of the rotors, causing catastrophic failure of the vehicle. While a fixed-wing aircraft can operate on a sloped landing strip by taking off traveling down the slope and land while traveling back up the slope, there is a need to provide a level and flat landing surface for VTOL aircraft.

This thesis discusses a semi-autonomous, mobile self-leveling landing platform designed to launch, recover and re-launch VTOL UAVs without the need for human

intervention. This system is self-powered and intelligent, allowing it to operate in remote or isolated locations with uneven terrain for extended periods of time. A literature review is performed for a number of existing UAV landing platform designs, self-leveling systems and previous research our group has performed on this topic. Specifically, this thesis discusses the most pressing issues regarding automated UAV launch and recovery systems, and the solutions that are employed to solve these problems in a cost-effective and straightforward manner.

The platform is not based on any commercially available mobile robots; instead it is designed, constructed and tested using a combination of open source and off-the-shelf components, as well as custom parts fabricated in-house. In contrast to other landing platforms, the vehicle presented here is designed and built to accommodate as many commercially available small-scale rotorcraft UAVs as possible thus maximizing its usability and versatility. This is accomplished this by using a landing surface that is not tailored for a specific aircraft, but rather is generic and suitable for many different UAV designs.

The contribution of this thesis resides in the presentation of a novel design of a mobile, self-leveling landing platform, a detailed description of the implementation of a prototype vehicle, and an experimental evaluation of its capabilities.

Related Work

This section provides a discussion of related research in two main areas: UAV / UGV collaborations and self-leveling systems. This section also contrasts the landing platform described in this paper with prior work from within our research group.

UAV / UGV Collaborations

A review of the literature surrounding this topic reveals a few examples of similar automated UAV / UGV systems. While these systems are designed to accomplish a set of functional objectives that are comparable to this landing platform design, to our knowledge, no existing system demonstrates the versatility and unique capabilities that this landing platform accomplishes.

The first notable example of a UAV / UGV collaboration, developed by the Space and Naval Warfare Systems Command (SPAWAR), is an automated UAV launch, recovery, refuel and re-launch system from an Unmanned Ground Vehicle (UGV) [1, 2]. The SPAWAR system, shown in Figure 1, incorporates a large, diesel powered, all-terrain UGV, which serves as an autonomous patrol vehicle as well as a base station for deploying a VTOL UAV. The SPAWAR system uses an Allied Aerospace iSTAR UAV, which is a 29-inch diameter ducted fan aircraft, powered by a piston-engine. Though both vehicles are high-performance, the UGV base station is heavy (weighing more than 3000 lbs. in most standard configurations [3]) and cannot level itself. Additionally, the UGV can only accommodate the iSTAR UAV, making its design specialized, and not generally adaptable.

Another example of a UAV / UGV collaboration system is discussed in [4]. This system uses an iRobot PackBot ground vehicle to coordinate target tracking with a Raven UAV when aerial reconnaissance and aerial tracking capabilities are required. Like the SPAWAR system, this system is based on a commercially available mobile robot designed to accommodate a single type of UAV. In this system, the Raven UAV does not

actually land on the PackBot, only collaborates with it. This limits its autonomous capabilities, because a human operator still needs to launch and recover the Raven UAV.

Fig. 1. SPAWAR UAV launch and recovery system [1-2].

Self-Leveling Systems

Another system is described in a patent for a self-leveling landing surface designed to allow helicopters to land on ships traveling in rough seas [5]. Normally, operating a helicopter from the deck of a ship is only possible during fair weather, and there have been several reported accidents involving helicopters attempting to land on ships that were rocking due to rough seas [6, 7]. The system incorporates a landing surface mounted on a

stack of rotating columns with angled mating surfaces and is designed to respond quickly to relatively small changes in the angle (high-frequency, low-amplitude), and cannot compensate for an angle greater than 15-degrees.

There are a number of designs for self-leveling systems presented in the literature. There are numerous potential applications for intelligent self-leveling systems, and as a result, these designs are not necessarily intended for use with UAVs or aircraft landing platforms. In [8], the focus is on building an autonomous, self-correcting platform using low-cost materials and hardware. The purpose of this work is to show that a self-leveling platform can be built quickly, with relatively low cost using common materials such as sheet metal, wood, door hinges, and plastic enclosures. It is actuated by standard RC servos, and controlled using an Arduino microcontroller that runs some basic electronics on a breadboard. This system is built for less than $100 USD, and demonstrates that a basic self-leveling mechanism does not need to be prohibitively expensive.

A cable-based self-leveling system intended to keep heavy cargo level during loading and unloading using a cable-driven mechanism is described in [9]. This system is intended specifically for leveling steel shipping containers that are commonly used aboard cargo ships and freight trains. Because the cargo inside these shipping containers is often valuable, it is important to keep them level to avoid shifting and damaging the contents. Unlike other self-leveling systems that are actuated from below, this design is controlled from above using cables, making it well suited for gantry cranes that transfer cargo at large shipping ports. This system uses a complex fuzzy logic controller to accomplish the task, and is expensive to implement. The presence of cables above the level surface makes it unsuitable for landing UAVs.

A conceptual design of a self-leveling system using an ATRV-Jr mobile robot as the base with a gimbaled landing surface mounted above is presented in [14]. This system uses a mechanism similar to a large universal joint to provide multi-directional flexibility with two Degrees of Freedom (DOF).

In contrast to these systems, the landing platform described in this thesis uses an integrated self-leveling system that compensates for the incline of whatever terrain it encounters, and can accommodate angles of 25-degrees in any direction (low-frequency, high-amplitude). Additionally, it can accommodate a number of different aircraft designs while remaining lightweight, compact, and relatively inexpensive to build. It accomplishes these goals without sacrificing off-road capabilities and long-term endurance in isolated locations.

Previous Work within the DU2SRI Group

The landing platform design described in this thesis is developed with the intention of addressing some of the limitations of the ISLANDS platform [12, 13] shown in Figure 2. Both platforms are developed with the same purpose in mind, to serve as a fully integrated ground station for UAV operations in remote locations. The ISLANDS platform is a large stationary unit that is designed to be driven from one location to the next on a truck. This mobility problem has been solved in the new landing platform design by making it into a mobile robot. ISLANDS also requires access to a source of electricity to recharge the batteries, which only last a few hours during constant operation. This means that a certain amount of human involvement is always required to keep the

ISLANDS platform operating, and many steps have been taken to minimize this dependency in the current landing platform design.

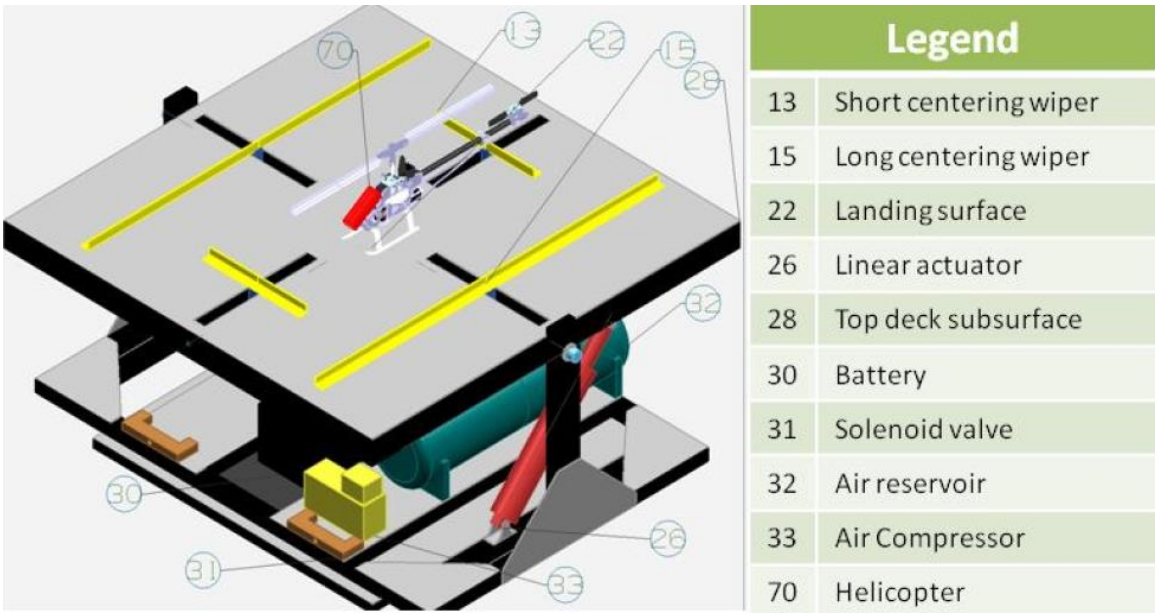

Fig. 2. The ISLANDS landing platform system [12-13].

The leveling system on the ISLANDS platform uses a basic two DOF design combining a DC gear motor for rotation about the central Z-axis, and a pneumatic linear actuator for changing the angle of the landing surface with respect to the platform's base. This system is capable of leveling itself on a slope using a two-step approach: (1) the ISLANDS platform rotates to align itself with the gradient, and (2) tilts the landing surface to match the angle of the slope.

The current mobile landing platform uses a more direct approach, leveling itself by adjusting the height of each corner individually using linear actuators, thereby changing the angle of the entire vehicle instead of just the landing surface. Its improved design does

not require an elevated landing surface, large actuators, or motors for central axis rotation, allowing the system to remain more compact and low-to-the-ground as needed for mobility. This new design also does not need to reorient itself to the slope before leveling.

CHAPTER 2: MECHANICAL DESIGN

Overview

The main requirements of the new landing platform design are its mobility and self-leveling capabilities. The basic configuration of the landing platform, shown in Figures 3 and 5, is a four-wheeled mobile robot with a differential drive system. The novel feature of this system is the combination of a conventional four-wheel design with an innovative self-leveling mechanism.

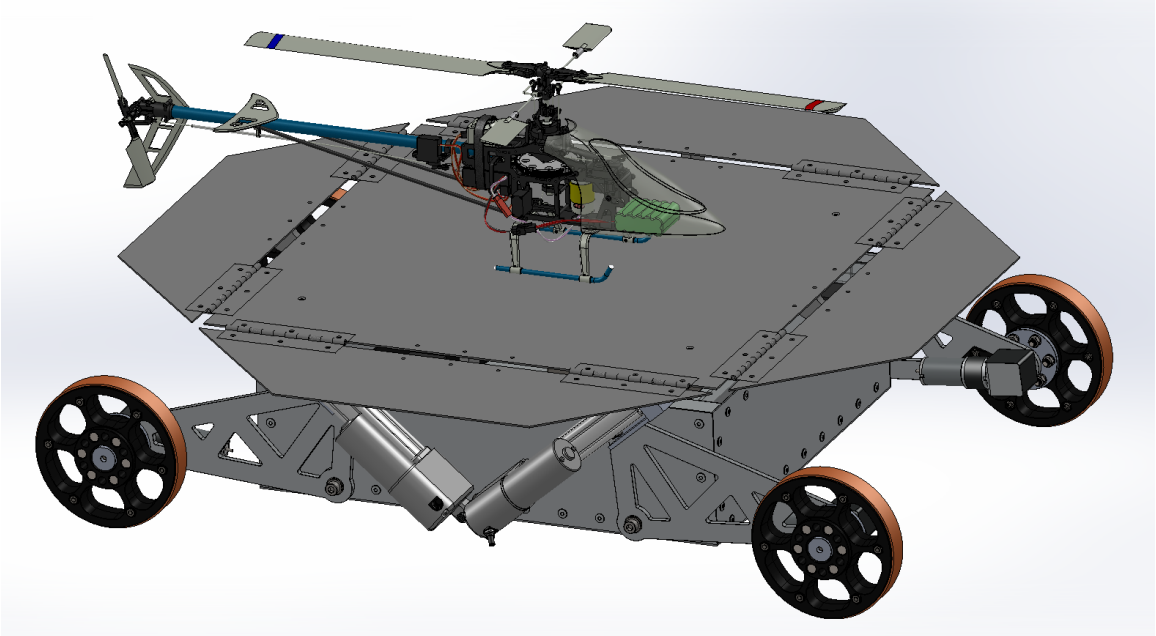

Fig. 3. SolidWorks model of the landing platform system.

Self-Leveling System

The self-leveling system of the landing platform provides its key functionality. One of the limitations of VTOL aircraft is that they cannot land on a sloped surface. Whereas a fixed-wing aircraft can take off and land traveling up or down a sloped runway because the lift is perpendicular to the direction of forward travel, a VTOL aircraft must have a flat landing area. This is primarily due to the physics of a rotorcraft whose lift is not dependent of the forward velocity of the aircraft. The lift produced by a rotorcraft comes from the downward thrust of the main rotor(s) as explained by Newton's Third Law of Motion, and this thrust is always parallel to the axis or rotation of the rotor(s) and perpendicular to the plane of the landing gear. To land a VTOL aircraft safely, the landing gear must be parallel to the landing surface; and if the surface is at an angle, the VTOL aircraft cannot make a controlled decent. Any attempt would mean that the lift produced by the VTOL aircraft would no longer be vertical and would carry the aircraft away from the slope at an equivalent angle. This will cause the aircraft to move in an unintended direction and possibly lose control. There is also the risk of a rotor strike when a rotor blade hits the ground, which would cause a catastrophic failure of the aircraft. Therefore, any VTOL aircraft must have a level surface to land on safely.

The self-leveling system allows the landing platform to adapt to its environment, and ensure a safe and level landing surface is always available to the VTOL UAV wherever it needs to operate. This system operates by changing the orientation of the entire landing platform vehicle mechanically by changing the height of each corner of the vehicle with respect to the ground. Like an automobile, the landing platform has four wheels, one at each corner of the vehicle. By raising or lowering the height of each wheel

independently, the landing platform can adapt to any slope up to 25 degrees regardless of its orientation. Forcing any of the wheels downward causes that corner of the landing platform to move upward. The mechanism for achieving this at each corner of the vehicle consists of three main components: a wheel, a control arm and a linear actuator.

Each of the four wheels is mounted on the end of a control arm that pivots about a fulcrum to rotate up and down and change the position of each wheel relative to the rest of the vehicle. The force that is required to move the control arm comes from an electromechanical linear actuator. Like a seesaw, the control arm is a lever rotating about a fulcrum, with the force of the vehicle's weight pushing one end of the lever up while the force of the linear actuator pushes on the other end. The linear actuator adjusts the position of the control arm and its corresponding wheel by extending and retracting, as shown in Figure 4. The ability to regulate the balance of forces acting on any individual control arm using the linear actuator is what allows for such precise control of the vehicle's landing surface. This gives the platform the ability to level itself on sloped or uneven terrain up to an angle of 25 degrees to within +/- one degree. The landing surface in this case is the top surface of the robot, which is an assembly of five stainless-steel flaps that measure a total 82.5 x 82.5 centimeters and form an octagon to better accommodate the area under the helicopter's main rotor(s). The design of the folding landing surface is described further in the "Folding Landing Surface" Section of this Chapter.

Fig. 4. Self-leveling mechanism of the landing platform.

The dimensions of the components in the self-leveling system are chosen based on the desired +/- 25 degree leveling requirement, along with the combined weight of the helicopter and landing platform and the force that can be expected during operation. The electromechanical linear actuators used on the landing platform are the Duff-Norton LT-100-1-100P models, shown in Figures 4 and 5. These linear actuators operate on 12 Volt DC, making them compatible with the onboard DC battery power that all of the landing platform systems operate on, as discussed in Chapter 3. The linear actuators are rated to deliver a continuous push-pull force of 500 Newtons (112 pound-force) over a 100 mm (4.2 inch) stroke length at a rate of 12 mm/sec. It should be noted that the actuators can

produce significantly more than the rated 500 N, but exceeding this load causes the actuator to move more slowly.

Fig. 5. Landing platform prototype with TREX 450 helicopter on board.

Given that the platform itself weighs approximately 18 kilograms, and the Align TREX 450 helicopter, shown in Figure 5, weighs just 900 grams, these linear actuators can provide sufficient force to lift the platform to the correct angle. Figure 6 shows the Free Body Diagram (FBD) of the control arm and actuator in the self-leveling system. In the FBD, F_{LAC} is the force provided by the linear actuator on the control arm, F_{WTE} is the

force provided by the wheel motor that can rotate inward to provide additional force at low transmission angles, and F_{LIFT} is the resulting lifting force that is being applied at the wheel to lift the corner of the vehicle. The angle between the linear actuator and the control arm is represented by θ (theta) which is the transmission angle, and the angle between the control arm and the ground is represented by φ (phi). As the linear actuator extends, the angle θ decreases and the angle φ increases. Because these two angles are dependent on one another, one can be written as a function of the other, as shown in Figure 7. The lifting force F_{LIFT} is dependent on these angles, and changes as the control arm moves through its range or motion, and this relationship is shown in Figures 7 and 8.

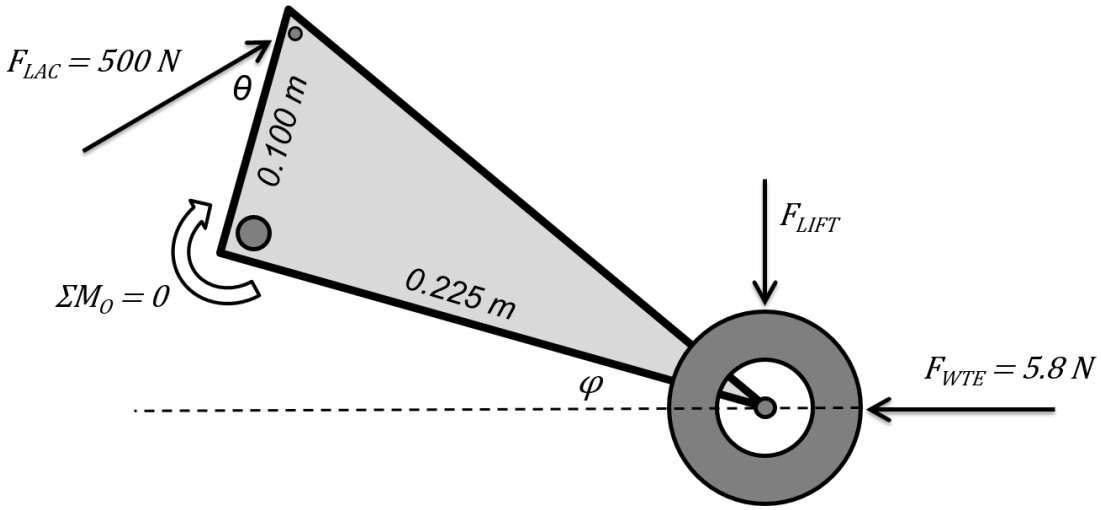

Fig. 6. Free body diagram (FBD) of self-leveling system.

The force balance of this system is based on the requirement that the sum of the moments about the pivot point, ΣM_o, is equal to zero. This requirement means that the force experienced by one side of the control arm is entirely dependent on the force being applied to the other side of the control arm. The force balance equations for this system

are shown in Figure 7 assuming that the landing platform is on flat ground. These force calculations also assume that the control arm is a rigid body, and does not deform under load. The stress analysis of the control arm design is discussed in more detail in later in this section. From Figures 7 and 8, it is evident that the self-leveling system can produce up to 189 N of lifting force at each wheel based on the rated force of 500 N from the linear actuators.

$$F_{LIFT} = \frac{0.1(F_{LAC}\sin\theta) + 0.225(F_{WTE}\cos\varphi)}{0.225}$$

$$\theta = -0.558\varphi + 53.049$$

$$-4.41° \leq \varphi \leq 76.48°$$

$$\therefore \quad 43.3N \leq F_{LIFT} \leq 188.9N$$

Fig. 7. Force equations for self-leveling system

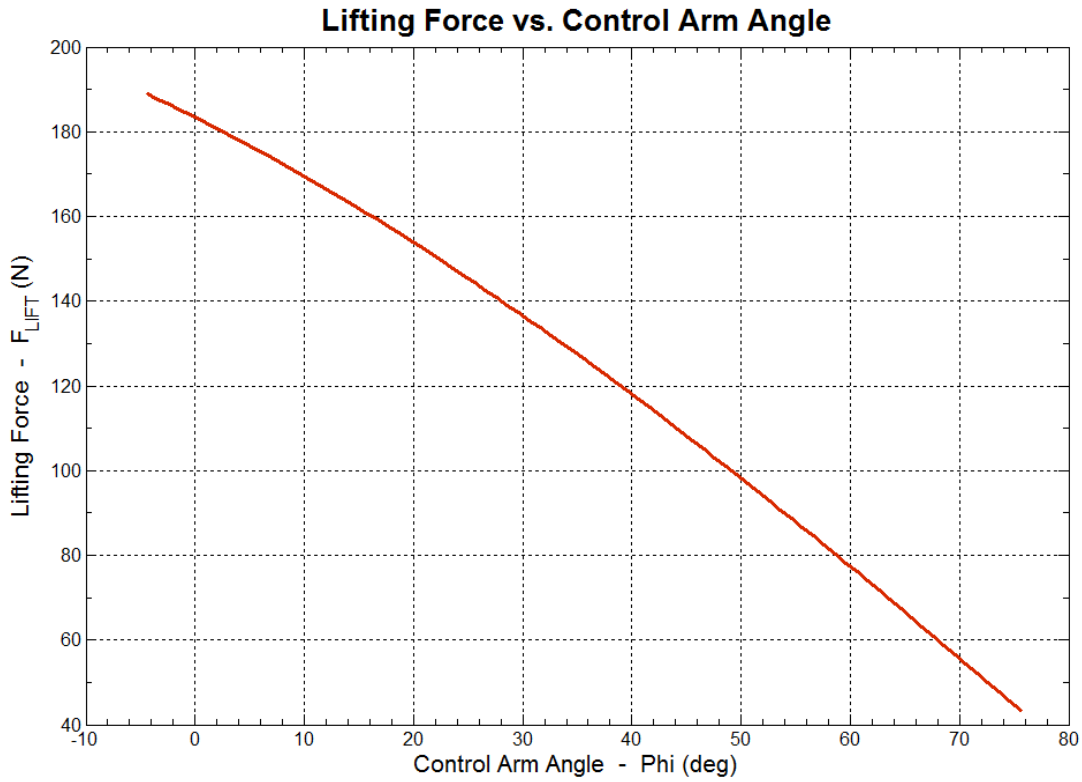

Fig 8. Plot of F_{LIFT} vs. control arm angle (φ) for self-leveling system

The linear actuators are individually controlled using four Firgelli Linear Actuator Controller (LAC) boards shown in Figure 9, which allow them to be operated like servomotors. Like a servomotor, the control signal dictates the desired position set-point of the linear actuator rather than the speed at which it moves. A 1.0 kHz Pulse Width Modulation (PWM) signal controls the position of each actuator through the LAC, which uses internal potentiometer position feedback to achieve the desired extension length. The potentiometer position feedback is built into the linear actuators, and functions by changing the electrical resistance (from 5 to 10 KΩ) between a reference wire and a signal wire depending on the amount of extension. A low voltage (3.3 Volts) is provided to the reference wire, and as the actuator extends the resistance decreases and the voltage at the

signal wire increases, according to Ohm's Law. The LAC reads the voltage at the position feedback signal wire, and determines how far in the actuator needs to extend or retract to reach the desired set-point set by the PWM signal. The duty cycle of the PWM signal can range from 0% to 100% which corresponds to a position set-point ranging from fully-retracted to fully-extended respectively.

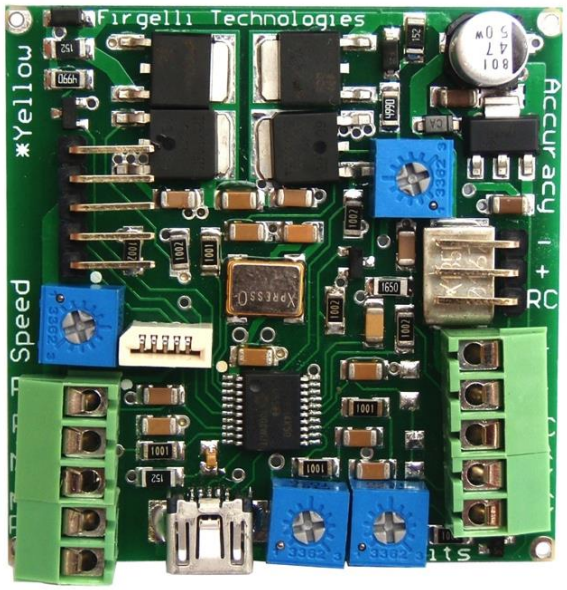

Fig. 9. Firgelli Linear Actuator Controller (LAC).

Each LAC is a fully-functioning stand-alone closed-loop controller, which handles all of the calculations necessary to reach the desired position and maintain that extension length until the PWM input signal changes. The LACs use a software based control algorithm, which allows all of the parameters of the controller to be tuned by the user from a computer via USB using the Firgelli LAC Advanced Configuration Software shown in Figure 10. This ability to tune each LAC individually to optimize the performance of its

companion linear actuator is essential when it comes to ensuring that the landing platform can remain within ± one degree of level. Although all four linear actuators are the same model from the same manufacturer, they do not all operate exactly the same right out of the box. This is primarily due to the fact that the potentiometer feedback is not identical in every linear actuator. For example, two identical actuators each connected to identical LACs and given the same 50% PWM signal should both extend to exactly 50 mm, however in reality one might extend to 51 mm and the other to 48 mm. This small discrepancy has a significant effect on the performance of the landing platform's self-leveling system and drive system, and tuning the LACs individually eliminates these types of problems.

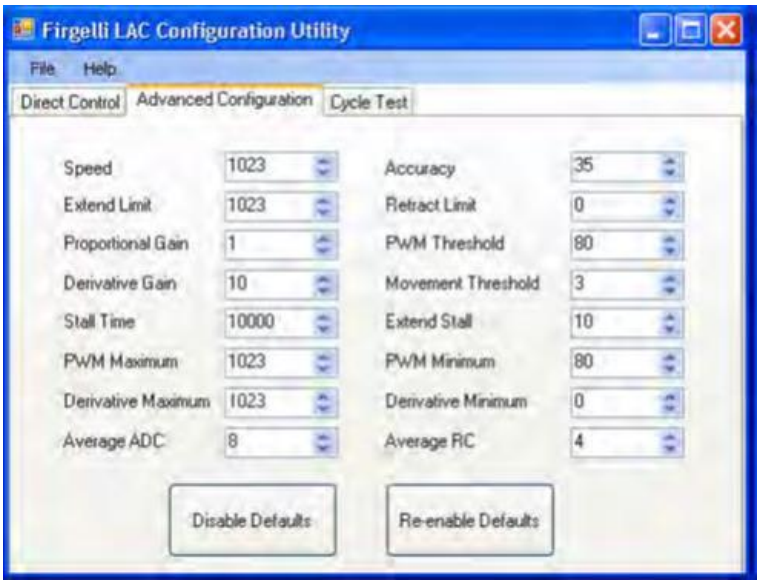

Fig. 10. Firgelli LAC Advanced Configuration Software.

The landing platform must be able to determine its present angle with respect to flat ground in order to level itself. The vehicle cannot be considered "self-leveling" unless it is able to automatically perform the leveling operation. The landing platform has two different methods for sensing its actual angle and determining what actuator movements will compensate for this angle. The sensor that provides the angle information for the self-leveling system is a Murata SCA121T analog dual-axis inclinometer, shown in Figure 11. The inclinometer measures the angles in the X- and Y-axes with respect to the direction of the Earth's gravitational pull. These readings can range from 0 to 180 degrees, with 90 degrees being considered perfectly level. On the landing platform, the angle of the X-axis corresponds to the incline between the front and back of the vehicle, and the Y-axis corresponds to the angle side-to-side. These angles are provided as a pair of linear voltage outputs from the inclinometer from 0 to 5.0 Volts. The voltage is proportional to the angle of that axis, and roughly equates to a sensitivity of 70 mV per degree. The voltage outputs from the inclinometer are converted into digital signals and sent to the landing platform's XMOS digital microcontroller, which is discussed in more detail in Chapter 3.

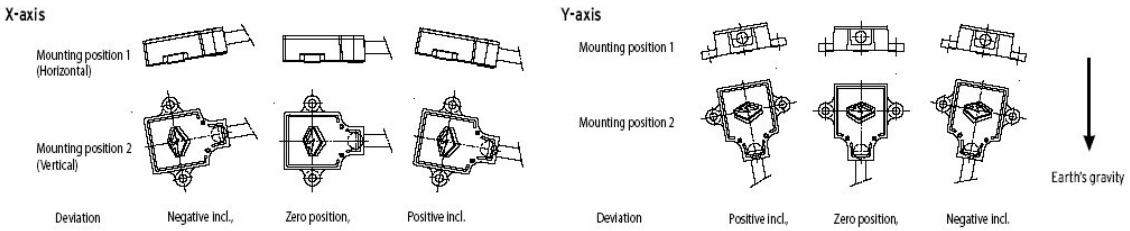

Fig. 11. Diagram of how the Murata SCA121T inclinometer measures angles [18].

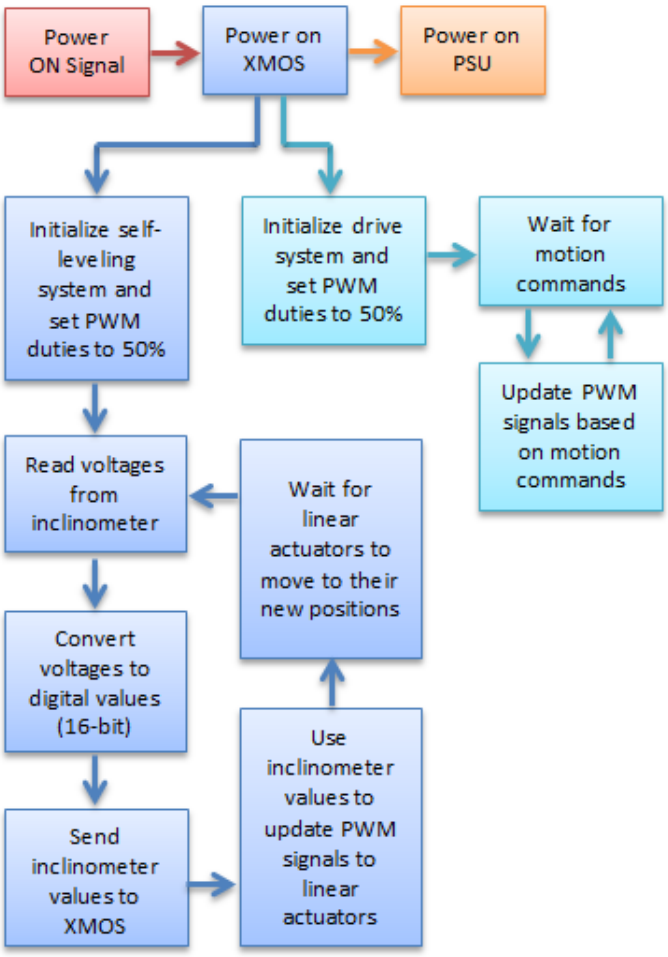

Fig. 12. Self-leveling system flow diagram.

Another source of information about the orientation of the landing platform comes from the analog position feedback signals from each of the four linear actuators. These signals are also converted from analog into digital signals and used to determine which actuators can be extended and which ones should be retracted to achieve the best level orientation. In some cases, raising one corner of the vehicle can produce the same effect as lowering the opposite corner of the vehicle. If one actuator is already near full extension (all the way up), the microcontroller can choose to lower that actuator rather than raise a

different corner. The results of the experimental testing of the self-leveling system, and an explanation of how the tests were performed are included in Chapter 4.

Although the primary function of the landing platform is to accommodate lightweight, unmanned helicopters, the platform is designed to be as rugged as possible without compromising its lightweight construction. It can be difficult to anticipate what kinds of loads the landing platform might experience in the field. The definition of a maximum loading condition is somewhat subjective, but for this project, it was defined as a 160 kg weight resting on top of the landing platform which is parked on a 15 degree side slope. This may seem like an unrealistic expectation, but one of the requirements of this project is that the landing platform meet U.S. Military performance expectations for similar sized robotic vehicles. Knowing that the military standards state that a 100 kg man can be expected to carry an average of 23 kg of gear on a daily basis, it is reasonable to expect the landing platform to endure being accidentally stepped on by a 123 kg person in the field.

The specific requirement is to accommodate a force of 392.4 N at each corner, which is equivalent to 160 kg evenly distributed to all four corners. The vehicle's structure must not sustain any permanent damage as a result of this load. This load condition is simulated using Finite Element Analysis (FEA) with two different independent models. The most important components in the vehicle's mechanical structure are the four control arms, and that is the focus of this discussion. The control arms are the components that transmit all of this force down to the ground, and they are the longest unsupported structural members. Because the control arms are only supported at one end, one of the goals of the FEA is to determine how much the unsupported end would deflect under the

maximum load. Any yielding of the material in the control arms is considered unacceptable and is the failure condition in this case. Yielding occurs when the material exceeds its yield strength and experiences plastic deformation, meaning that it bends so much that it will never return to its original shape when the load is removed. In the case of the 6061-T6 aluminum alloy chosen for the control arms, yielding is followed closely by complete failure due to the alloy's tendency to crack abruptly.

The control arm is analyzed using FEA models in two different software packages. The purpose of this parallel analysis is to verify that the results produced by the two models match up correctly. To avoid relying on a single model which could have produced overly optimistic results, the control arm geometry was analyzed in both SolidWorks SimulationXpress and Abaqus CAE. Both models apply fixed boundary conditions to the locations at which the control arm attaches to the vehicle body and the linear actuator. These locations are defined as the contact surface between the control arm and the ball bearings to which the components mount to, as shown in Figure 13 by the green arrows. The fixed boundary condition that both models use is known as an "encasture" condition, which restricts movement in all six DOFs (all translational and rotational movement) at the nodes where the boundary condition is applied.

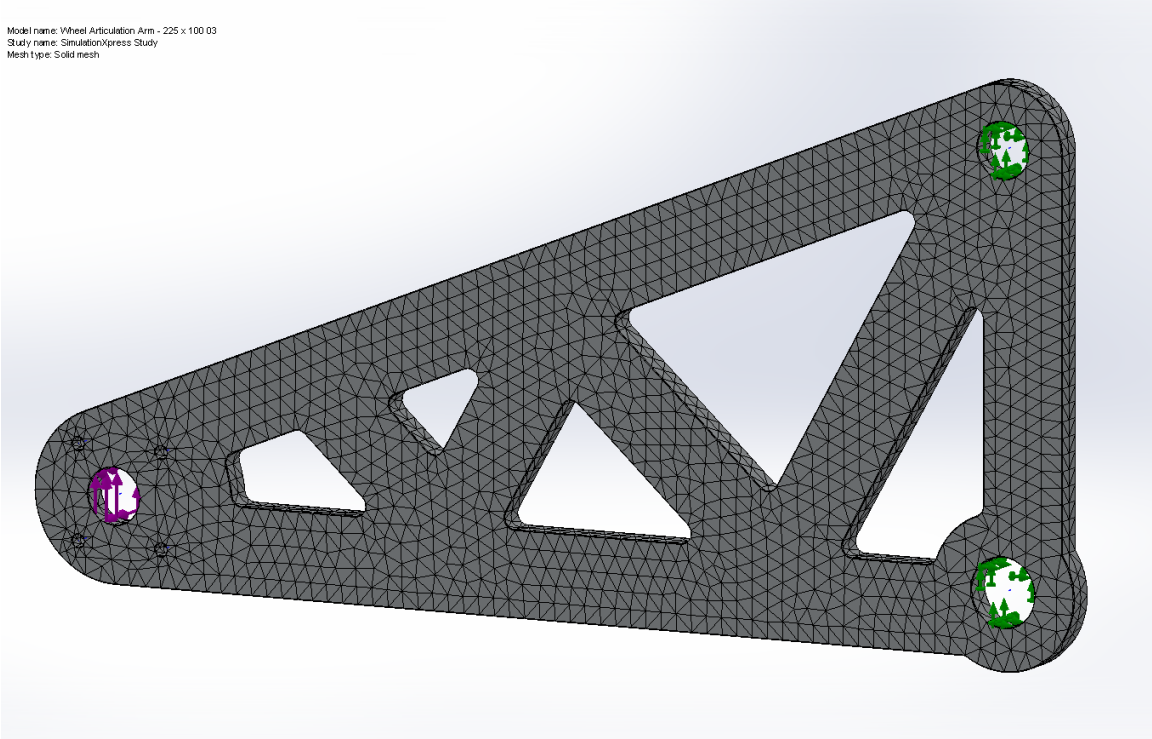

Fig 13. Control arm FEA boundary conditions and loads.

The forces that simulate the maximum load condition are applied to the contact surface of the wheel bearing at the unsupported end of the control arm. These forces consist of a horizontal and vertical force component, and a wheel offset moment, all shown in Figure 13 by the purple arrows. The magnitude of these force components come from the equations in Figure 14, which are the loads that occur during the maximum load condition. These forces are based on the 392.4 N force acting at a 15 degree angle. The torsional moment comes from the wheel being offset to one side of the control arm, because all of the force must be transmitted through the wheel to the ground. The loads are applied incrementally over ten intervals in the simulation in the form of a ramp function. This means during that each increment, the loads increase by 10% of their final value.

$$Horizontal\ Force\text{:}\ F_H = 40\ kg \cdot (9.81\ m/s^2) \cdot \sin(15°) = 101.561\ N$$

$$Vertical\ Force\text{:}\ F_V = 40\ kg \cdot (9.81\ m/s^2) \cdot \cos(15°) = 379.029\ N$$

$$Wheel\ Offset\ Moment\text{:}\ M_{WT} = \frac{101.561\ N}{0.076\ m} = 1336.3\ N \cdot m$$

Fig. 14. Equations of forces applied in FEA models.

So far, both the Abaqus and the SolidWorks FEA models have followed all of these parameters in a similar way. The primary differences between the two models are the meshes. While SolidWorks does not allow for any mesh refinement or customization of the model to better reflect the real world conditions, Abaqus has more tunable parameters. The mesh in SolidWorks FEA is generated automatically and the user has no control over what elements will be used and how fine or coarse the mesh will be. SolidWorks uses the 4-node linear tetrahedron element (TET4) in every model, which is computationally inexpensive and easier to mesh. The problem is that this element is too stiff in bending because it has a constant strain over the characteristic length of the element. Because this model is simulating loads that are causing the control arm to bend, the TET4 mesh can be expected to produce stresses which are artificially low. Regardless, this SolidWorks FEA model can still determine whether the part is going to be close to failure, and it takes very little time to run this model. This makes it easy to change the control arm design and rerun the FEA model if necessary.

The SolidWorks FEA calculated the maximum stress to be 149.1 MPa using the von Mises equivalent stress calculation method, as shown in Figure 15. Von Mises equivalent stress is a method of combining stress components occurring in a multi-axial stress problem into a single numerical value. If the von Mises stress exceeds the material's yield

strength (275 MPa for this 6061-T6 aluminum alloy) the part has yielded. The SolidWorks FEA model shows that the maximum stress under this loading condition is only 54.2% of the yield strength, resulting in a safety factor of 1.844. Again, these results can be expected to be artificially low due to the stiff TET4 mesh, but it is clear that this control arm design is not going to fail under these conditions.

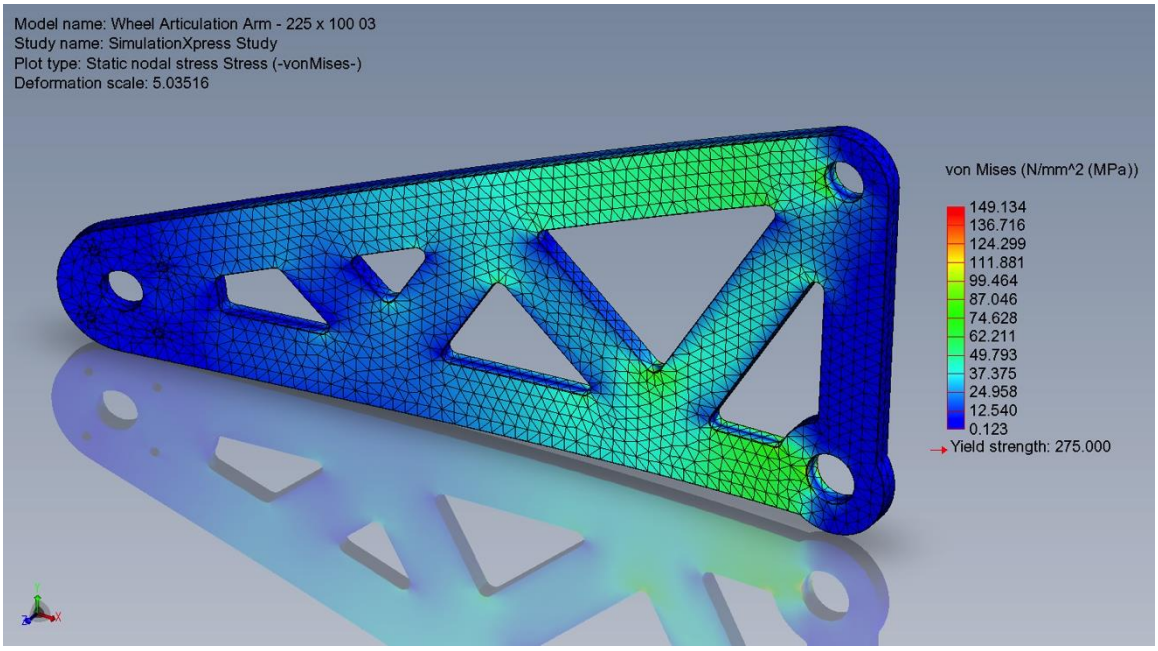

Fig. 15. Control arm von Mises equivalent stress contour plot from SolidWorks FEA.

After establishing that the control arm design was not likely to fail, the next step is to verify the SolidWorks results using a more time consuming and computationally expensive Abaqus FEA model. Unlike SolidWorks which is a 3D modeling software that includes an FEA toolbox, Abaqus is a purpose-built FEA software package. Abaqus requires the user to specify every detail of the analysis, which is time consuming but more reliable if the model is setup correctly. The primary difference in the Abaqus model was

the use of a custom mesh that was refined to be as accurate as possible while still computationally efficient. The mesh in the Abaqus model uses the 8-noded hexahedral element (HEX8) which is better in bending than the TET4 element. A HEX8 mesh is more computationally expensive, but provides more realistic results under these conditions.

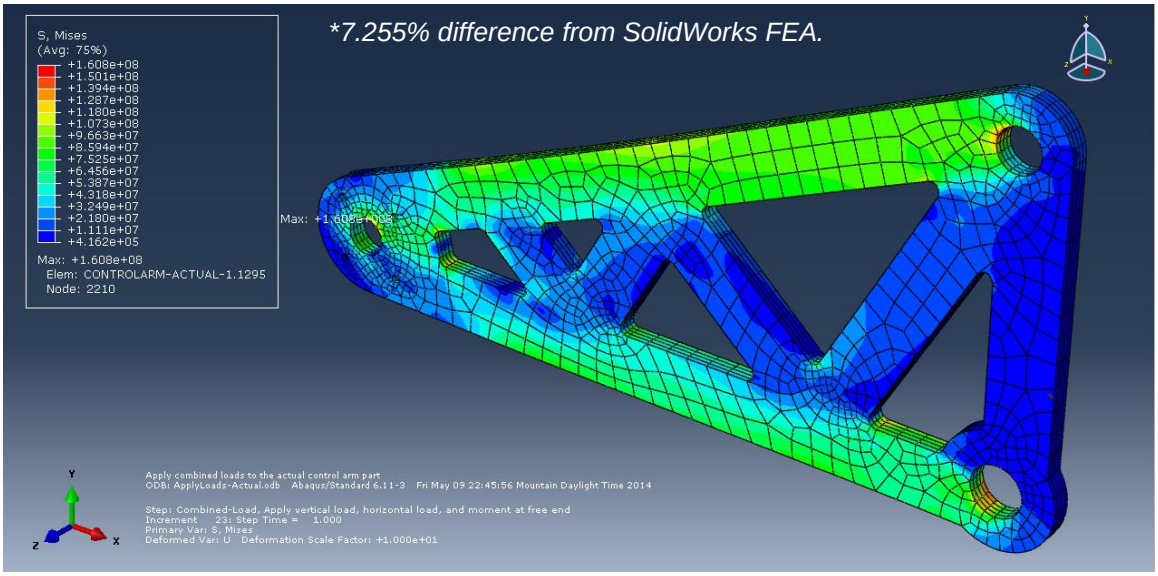

Fig. 16. Control arm von Mises equivalent stress contour plot from Abaqus FEA.

The Abaqus FEA model calculated the maximum stress to be 160.8 MPa, again based on the von Mises equivalent stress, as shown in Figure 16. As expected, this refined mesh produced a result that is larger, and likely more realistic than the SolidWorks FEA model. The Abaqus calculated maximum stress is 7.255% greater than the value from the SolidWorks model. Another equally important calculation was the deflection of the unsupported end of the control arm where the loads were applied. If the deflection is more than a few millimeters, it could create interference issues between the control arm and the vehicle's body or the linear actuator bracket. The Abaqus FEA model calculated the

maximum deflection magnitude at the tip of the control arm to be 1.62 mm (0.064 inches), as shown in Figure 17. This deflection is small in comparison to the thickness and length of the part, and does not cause any interference issues.

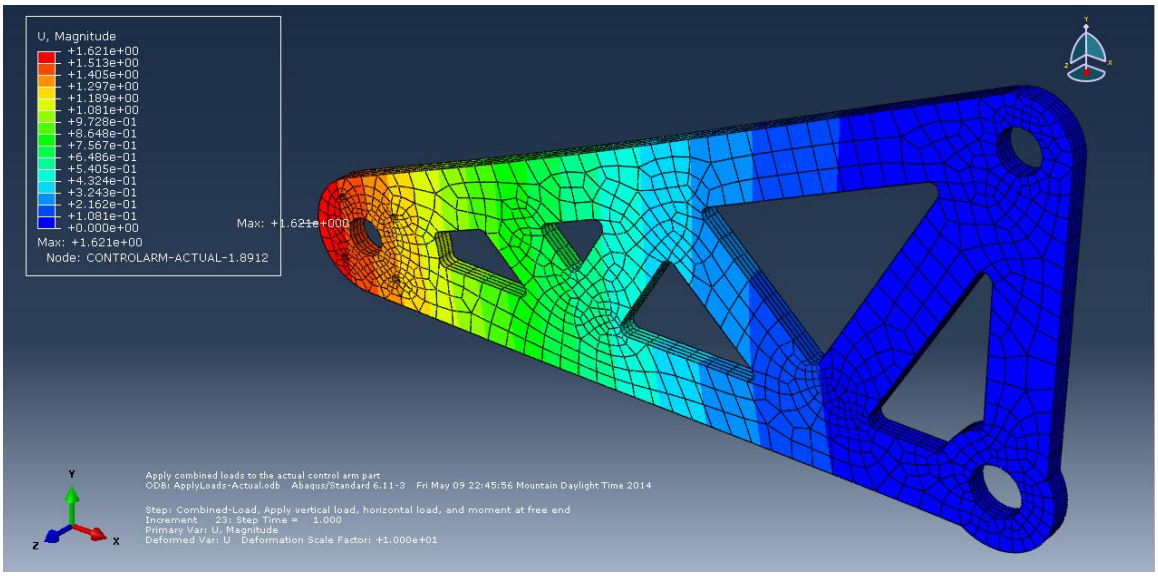

Fig. 17. Control arm deflection magnitude contour plot from Abaqus FEA.

Drive System

In addition to the self-leveling system, another important consideration in the landing platform's mechanical design is the drive system. This is what gives the landing platform mobility. The drive system is based on a four-wheel differential drive architecture. In this system, each wheel is driven by its own 24 Volt DC gear motor, giving the vehicle a true four-wheel-drive system, as shown in Figure 18. The wheel motors feature right-angle gearboxes, allowing them to mount tightly up against the control arms. These wheel motors are individually controlled, allowing them to move in different directions if necessary. This is the basis for the vehicle's differential drive

system, in which the wheels on one side of the vehicle rotate in the opposite direction from those on the other side of the vehicle. This causes the vehicle to rotate in place, giving it the tightest possible turning radius.

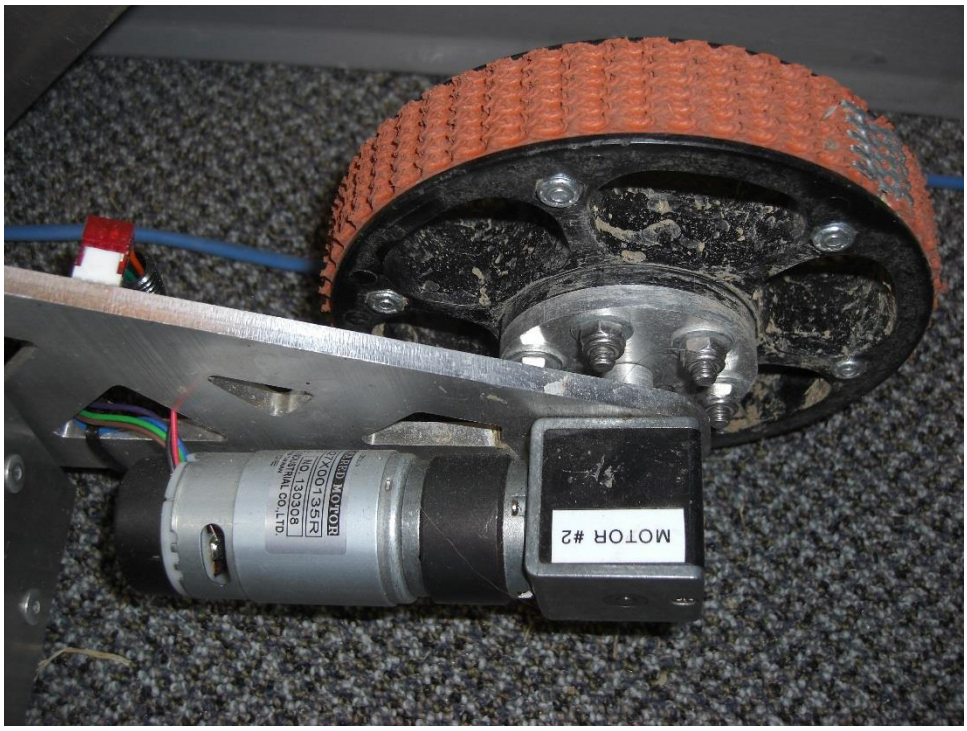

Fig. 18. Wheel motor and wheel mounted to the control arm.

The requirements for the drive system state that it must be able to move the vehicle at a speed that is approximately walking pace. This was defined as a maximum speed of at least 1.4 m/s (5.0 km/h). The rated speed of the wheel motors is 192 rpm at the rated load of 441.3 mN-m. With the wheels shown in Figure 18 that have a 152 mm (6 inch) diameter, the calculated maximum speed of the vehicle is 1.52 m/s (5.46 km/h). This calculation suggests that the chosen drive motors fulfill the speed requirement. An experimental evaluation of the vehicle's drive system is provided in Chapter 4.

The drive system, like all of the landing platform systems, needs some form of self-awareness. The drive motors are each equipped with a two-channel Hall Effect encoder that sends pulses to the digital microcontroller. The frequency of these pulses is directly proportional to the speed of the motor. The pulses on the two channels are 90 degrees out of phase with one another, allowing the microcontroller to also determine the direction of rotation of each wheel motor. A sample of a wheel encoder signal is shown in Figure 19. The data from the wheel encoders allows the microcontroller to detect if any of the wheels are slipping or stalled, indicating a problem that may require shutting down one of the drive motors.

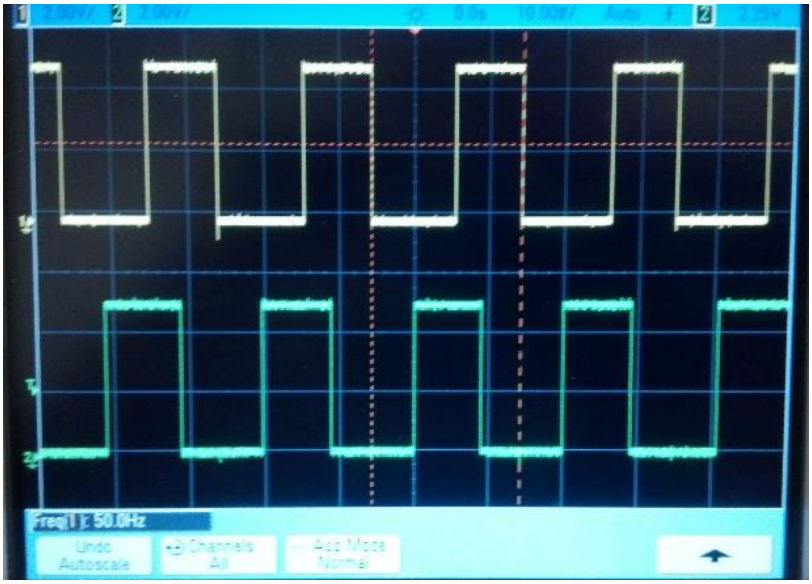

Fig. 19. Wheel encoder signal while rotating at 10% power.

Folding Landing Surface

Another design requirement is for the platform to be carried on the back of an average person. Guidelines for these requirements come from other civilian/military robots being carried into the field, notably the PackBot EOD which can be carried and easily deployed by a soldier [15]. The PackBot EOD weighs approximately 18 kilograms, which according to studies by the US military, is below the maximum amount of total weight (23 kilograms) that an average person can safely carry over long distances without experiencing premature exhaustion [16]. As a result, the landing platform is designed with a similar target weight limit of 18 kilograms. Another feature of the PackBot is that it can be reduced to a compact configuration by rotating its extendable tread arms inward to sit beside the vehicle's body. Similarly, the landing platform is designed with a collapsible landing surface which folds up into a more compact and more durable configuration for transport, as shown in Figure 20. It accomplishes this by rotating the four trapezoidal flaps 180 degrees inward so that they rest flat on the center section. In this configuration, the landing platform vehicle measures 55 centimeters wide, which is compact enough to be carried on the back of a person without impeding movement.

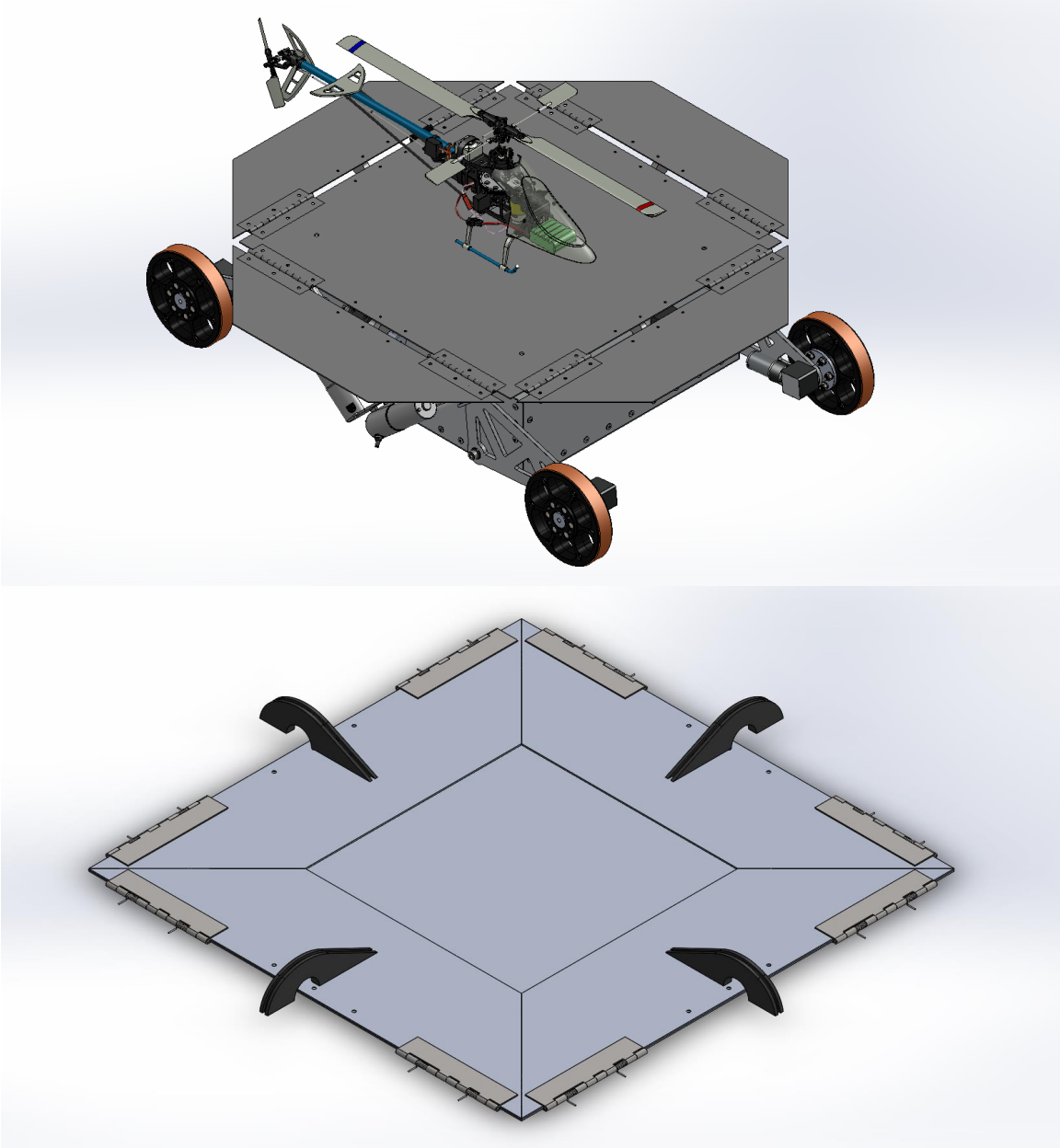

Fig. 20. Extended and folded landing surface configuration.

The folding landing surface, as shown in Figure 21, uses eight spring-loaded stainless steel hinges that force the four flaps closed. To make this system fully automatic, the landing surface uses a motorized cable operated mechanism to pull the landing surface open. This mechanism uses four miniature winches to pull each cable

over a cam at the edge of the landing surface, as shown in Figure 22. Each of the four winches has a maximum pulling force of 267 N (60 lbf), and they are not back-drivable by the spring-loaded hinges. This means that the landing surface is held open without the motors requiring any power. Only when the motors are reversed, is the landing surface allowed to close.

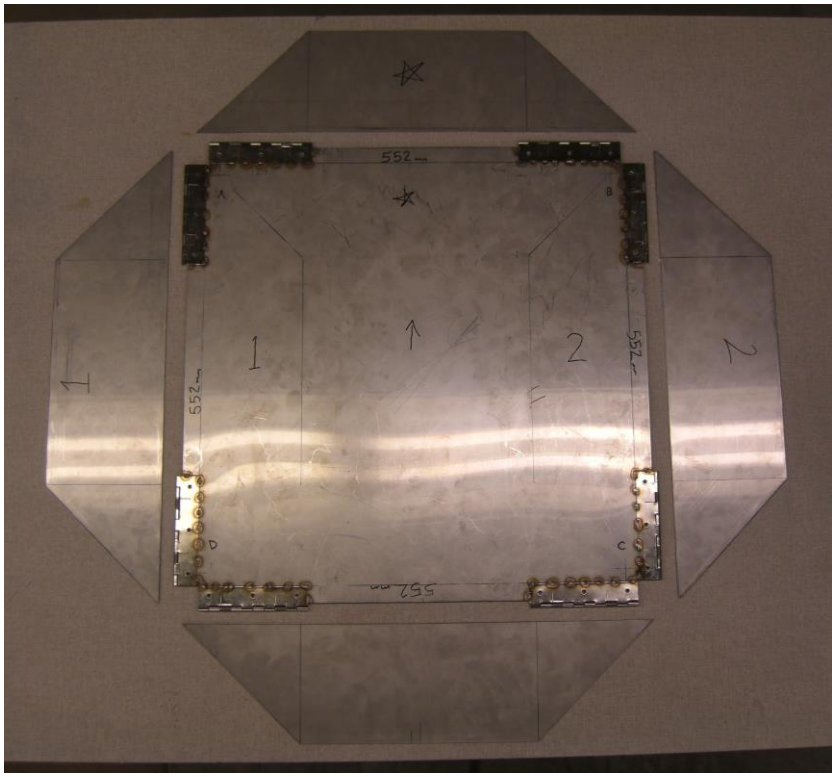

Fig. 21. Welded stainless steel folding landing surface.

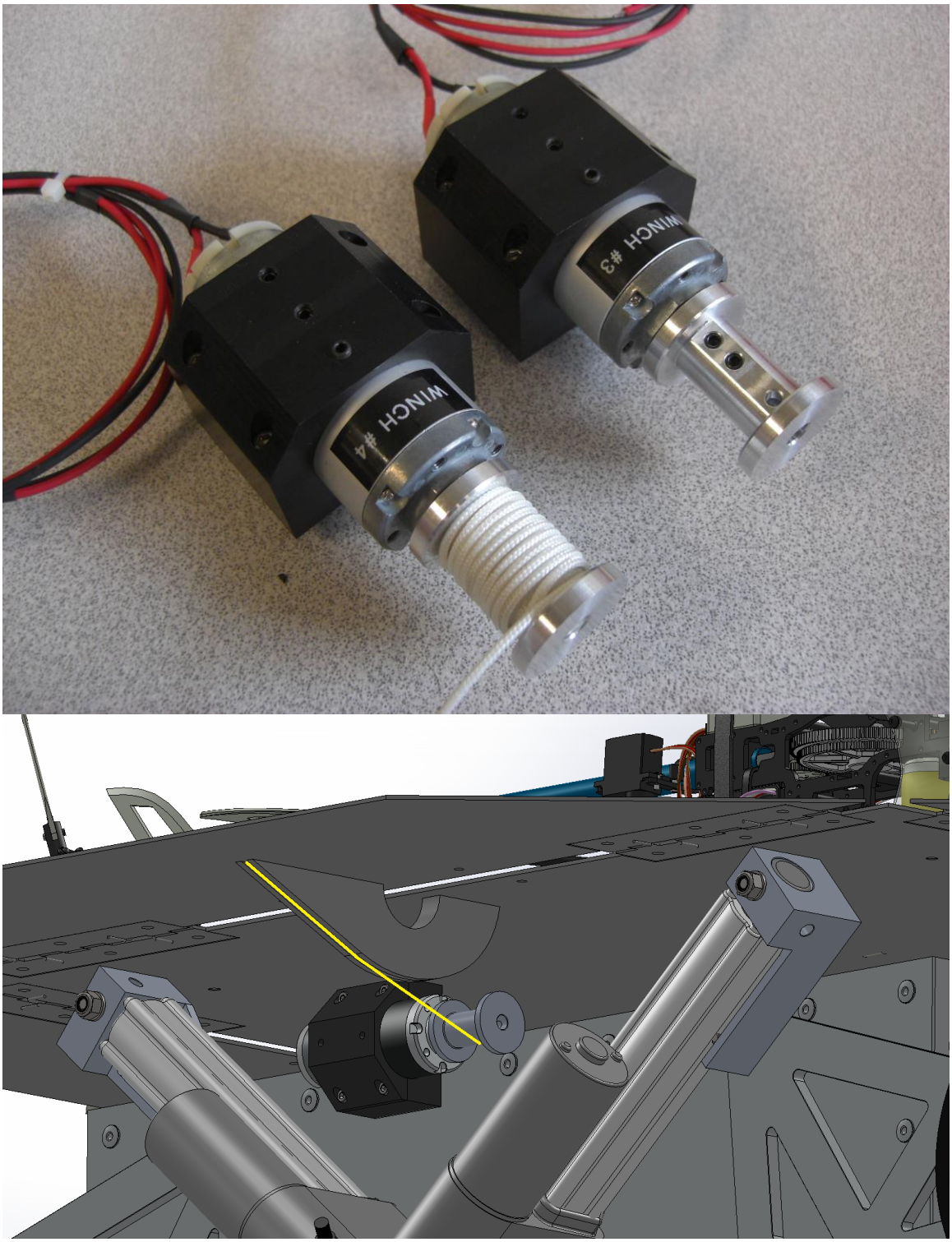

Fig. 22. Cable operated unfolding mechanism.

CHAPTER 3: ELECTRICAL AND SOFTWARE DESIGN

Overview

The landing platform is not only a place to land for UAVs, but it is also a mobile robot and a remote sensor platform. Like any mobile robot, the landing platform relies on an integrated network of power electronics, batteries, sensors, wireless communication and digital controllers. In this chapter, the electrical design of the landing platform is described in detail. This discussion is broken down into four sections, The Power Distribution System, the Solar Recharging System, the Control, Communication and Sensor systems, and the Software. These electrical systems provide the energy to operate the mechanical components, and they give the landing platform the ability respond to operator commands as well as make autonomous decisions. The landing platform is not just a remote controlled robot, but an intelligent, self-aware, semi-autonomous vehicle which can perform many of its duties with minimal intervention from a human operator.

Power Distribution System

One of the primary electrical design considerations is how to power all of the onboard systems. This includes understanding how much stored electrical energy the landing platform can carry onboard, how to distribute the power to the various electronics and motors, and how to keep the power systems as efficient and lightweight as possible. This begins with the batteries, which are critical to the performance and endurance of any

mobile robot. To provide some comparison, the iRobot PackBot EOD mentioned in Chapters 1 and 2, which is similar in size and weight to the landing platform, uses a lithium battery pack with a total onboard energy capacity of 500 Watt-hours. Like the PackBot, the landing platform is required to travel long distances over rough terrain and operate for extended periods of time in the field. Therefore it was decided that the landing platform should have an onboard energy storage capacity that is similar to, and if possible, larger than that of the PackBot.

After an analysis of the expected power consumption of the landing platform prototype vehicle, a battery system was chosen that allows the vehicle to operate for several days if necessary on battery power alone. Four lithium-polymer battery packs were selected to power the landing platform prototype vehicle, providing a total onboard energy capacity of 814 Watt-hours. These battery packs are waterproof 5-cell (5S) 18.5 Volt 11,000 mAh with a 440 Amp maximum discharge rate manufactured by MaxAmps in Washington. One of these battery packs is shown in Figure 23. The 814 Watt-hour capacity provides enough power for the platform to remain in the field for several days, or travel a distance up to 48 kilometers (in ideal conditions) without requiring recharging. A breakdown of the average power consumption for each of the electrical components of the landing platform is shown in Table I. Based on the data in this table, it is possible to calculate how long the batteries will last while performing different operations.

Table I. Breakdown of power consumption of the prototype vehicle

Component	Consumption	Activity Level
XMOS XC-1A Microcontroller	5.0V*500mA	Always Active
WiFly Module	3.3V*210mA	Always Active
Control Electronics Power =	**3.193 Watts**	**Always Active**
LTC1865 ADC (x2)	5.0V*2mA	During Leveling
SCA121T Inclinometer	12V*8mA	During Leveling
Duff-NortonLT-100-1-100P (x4)	12V*1500mA	During Leveling
Self-Leveling System Power =	**72.116 Watts**	**During Leveling**
GPS Module	5.0V*50mA	During Locomotion
Wheel Motor Encoders (x4)	3.3V*5mA	During Locomotion
IG-32PGM Wheel Motors (x4)	21V*1000mA	During Locomotion
Drive System Power =	**84.316 Watts**	**During Locomotion**
IG-32 Landing Surface Motors (x4)	12V*400mA	During Unfolding
Folding Landing Surface Power =	**19.200 Watts**	**During Unfolding**

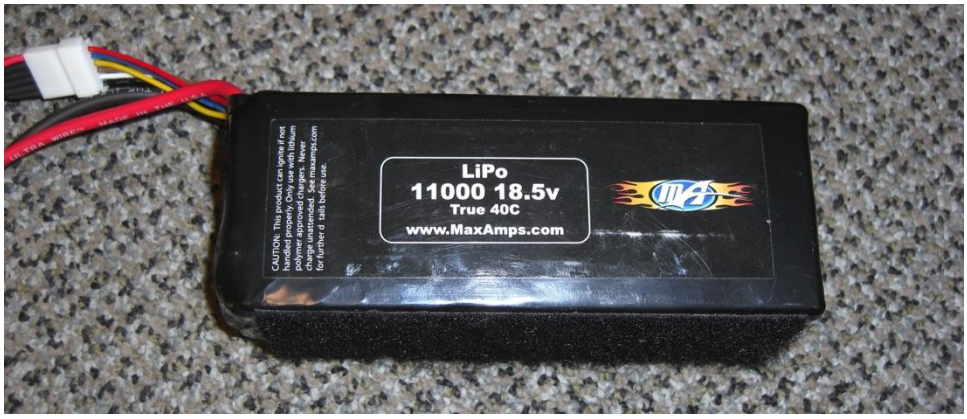

Fig. 23. MaxAmps 5S 18.5 Volt 11,000 mAh lithium-polymer battery pack.

When fully charged, the battery packs provide 21.0 Volts, however the only components on the landing platform which operate directly on the battery voltage are the wheel motors. All of the other components require a lower voltage, so it is essential that the landing platform includes a system for stepping-down the battery voltage to the levels that are required by the other components. In order to efficiently distribute the power among the various electrical components the landing platform prototype uses a multiple-

output 250 Watt DC-DC converter shown in Figure 24 that takes the battery voltage (18.5-21.0 Volts) and steps it down to four different levels, +3.3 Volts, +5.0 Volts and +/- 12 Volts. All of the other electrical components, such as the linear actuators, sensors, wireless communication and the digital microcontroller use one of these four voltages to operate. This DC-DC converter system runs at 95% efficiency under normal operating conditions under 50% of the maximum load. A schematic of the power distribution system through the DC-DC converter is shown in Figure 25. The output labeled +5 VSB in the schematic provides 5.0 Volts for the XMOS digital microcontroller and the WiFly wireless communication module at all times. All of the other voltage outputs are controlled by the digital microcontroller, and can be deactivated to conserve power when they are not in use.

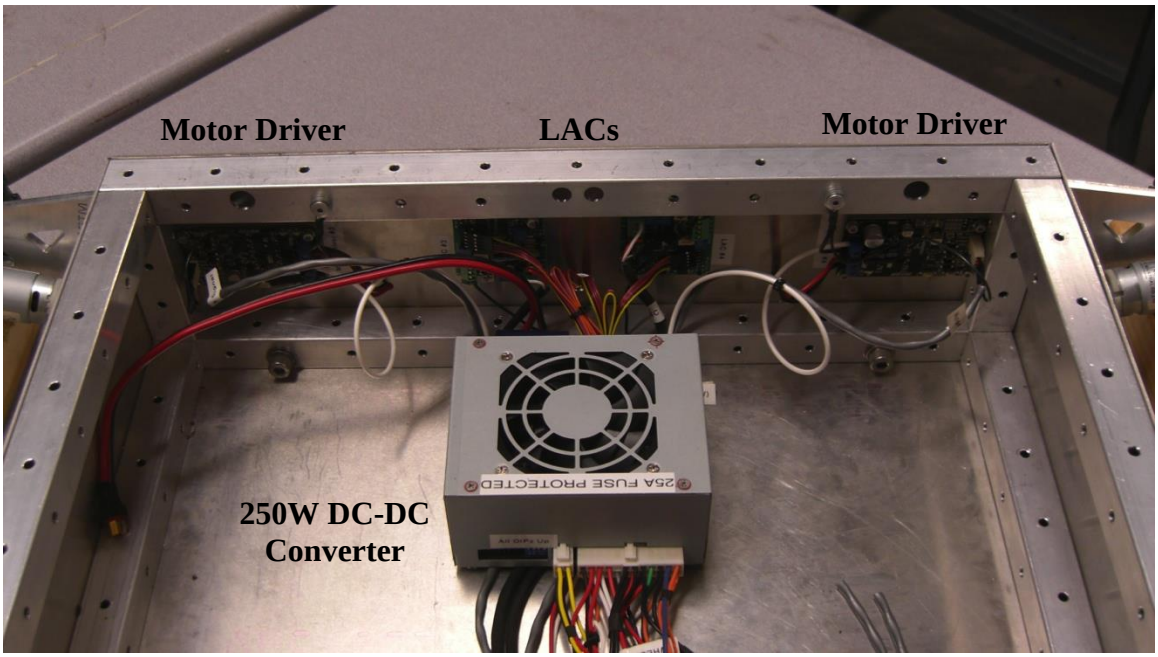

Fig. 24. DC-DC converter, LACs and motor drivers.

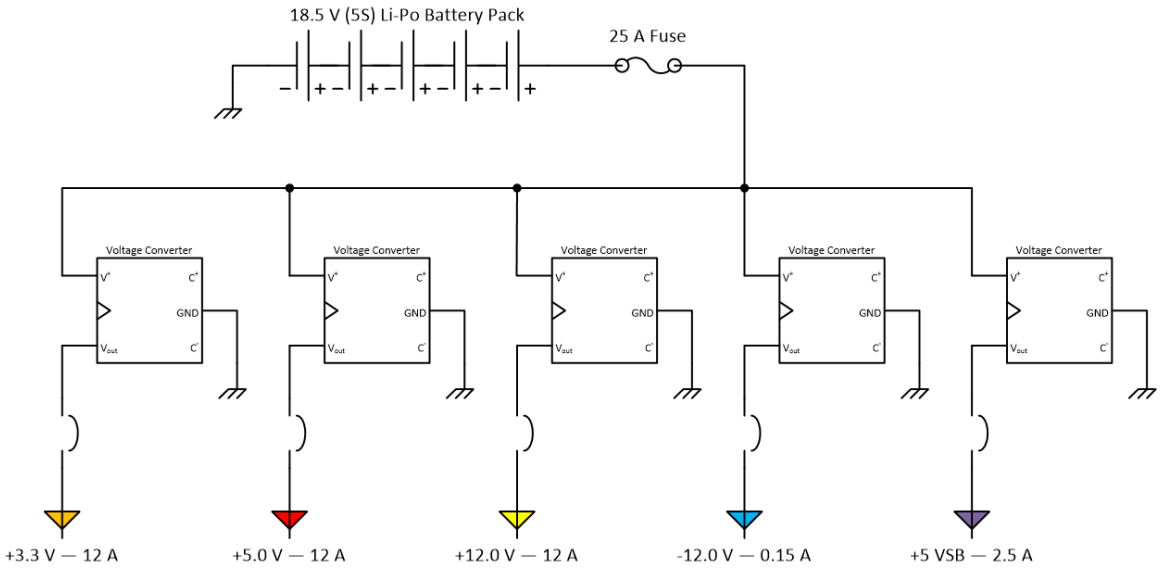

Fig. 25. Schematic of the power distribution system through the DC-DC Converter.

The other components that are shown in Figure 24 are the wheel motor drivers and the LACs. These components are part of the power distribution system as well because they are responsible for taking the low-voltage PWM signals from the XMOS digital microcontroller and converting them into high-voltage high-current signals that the motors and actuators operate on. The wheel motors each require 18.5-21.0 Volts up to 5.0 Amps, and the linear actuators each require 12 Volts up to 3.5 Amps. The motor drivers and LACs serve to isolate the sensitive microcontroller from these high power levels while still allowing it to control the motors and actuators. Similar motor drivers are used for the folding landing surface motors, and serve the same purpose.

All of the electrical components, including the motors, actuators, batteries, sensors, and digital microcontroller share a common ground. This means that while the different components may be powered from different positive voltages, they are all interconnected to the same (negative) ground. Automobiles also use this common-ground architecture, in which the chassis of the car acts as the ground for all of the electronics. Similarly, the landing platform uses its aluminum alloy structure as the ground for all of the components.

Using a common ground for all of the components greatly simplifies the electrical design of the landing platform in two ways. First, it eliminates almost half the wires which are required to provide power to the numerous components. Instead of having to run both a positive and negative power connection all the way from the DC-DC converter to every component, only the positive power connections are necessary. All of the negative power connections are attached directly to the aluminum chassis of the vehicle, as shown in Figure 26. The second advantage of a common ground is the stability of the low-voltage control signals. Because the control signals are so sensitive to small fluctuations, having separate grounds could cause malfunctions. By ensuring that all of the components have the exact same reference voltage via a common ground, it guarantees that the low-voltage signals are perceived the same way by the sending device and the receiving device.

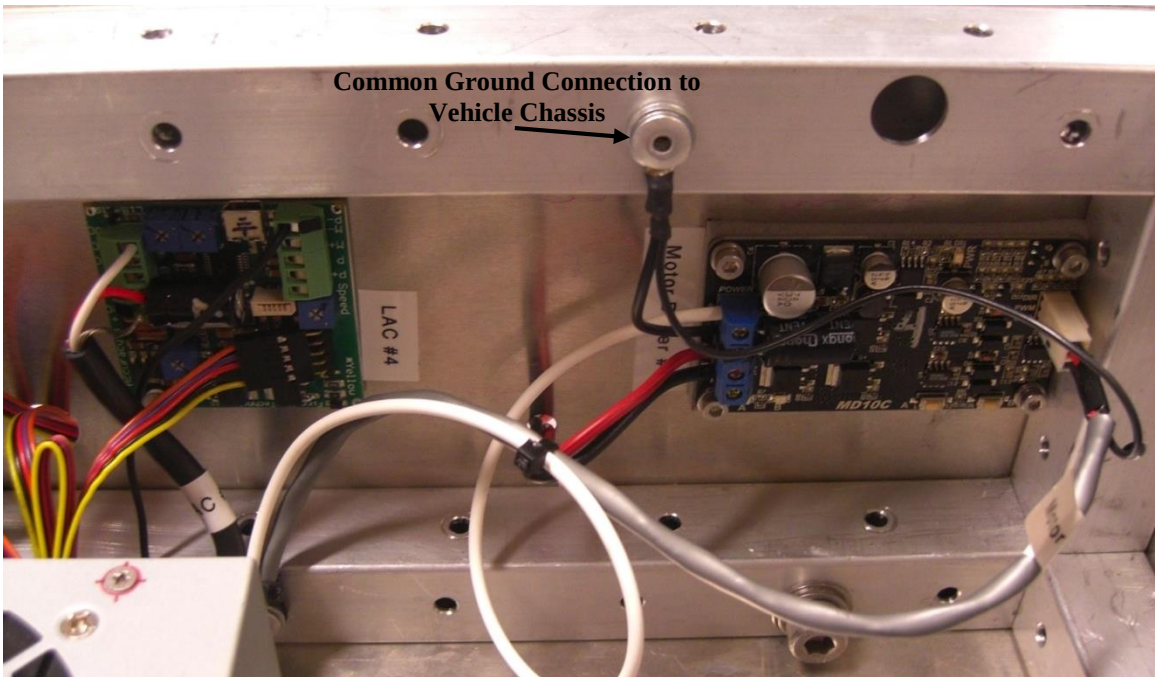

Fig. 26. The common ground connection of an LAC and a motor driver.

Solar Recharging System

One of the design requirements of the landing platform is to allow it to remain out in the field for extended periods of time with minimal human intervention. As discussed in the previous section, the landing platform carries a large amount of stored electrical energy onboard in the form of rechargeable lithium-polymer battery packs. While these batteries can power the vehicle for several days if necessary, they will eventually need recharging. Because the landing platform is designed to operate in isolated or inaccessible locations, recharging the batteries using traditional methods, such as an AC powered battery charger, is impractical and unrealistic. To solve this problem without requiring a human operator to travel to the vehicle's location and recharge the batteries, a solar powered recharging system has been developed for the landing platform.

The solar charging system that has been developed for the landing platform makes use of the large surface area on the top of the vehicle. The landing surface when fully extended measures more than 6428 square-centimeters (996 square-inches), which offers a lot of potential for capturing solar energy. According to NASA data, on an average day in May in Denver, Colorado, 6.11 kilowatt-hours of solar radiation energy are transferred to every square-meter of surface area [19]. Based on this statistic and the surface area of the landing surface, an average of 3928 Watt-hours of solar radiation energy is transferred to the landing surface every day assuming 100% efficiency. Remembering that the onboard battery capacity of the landing platform is 814 Watt-hours, the solar radiation energy reaching the landing surface is substantial and worthwhile trying to capture.

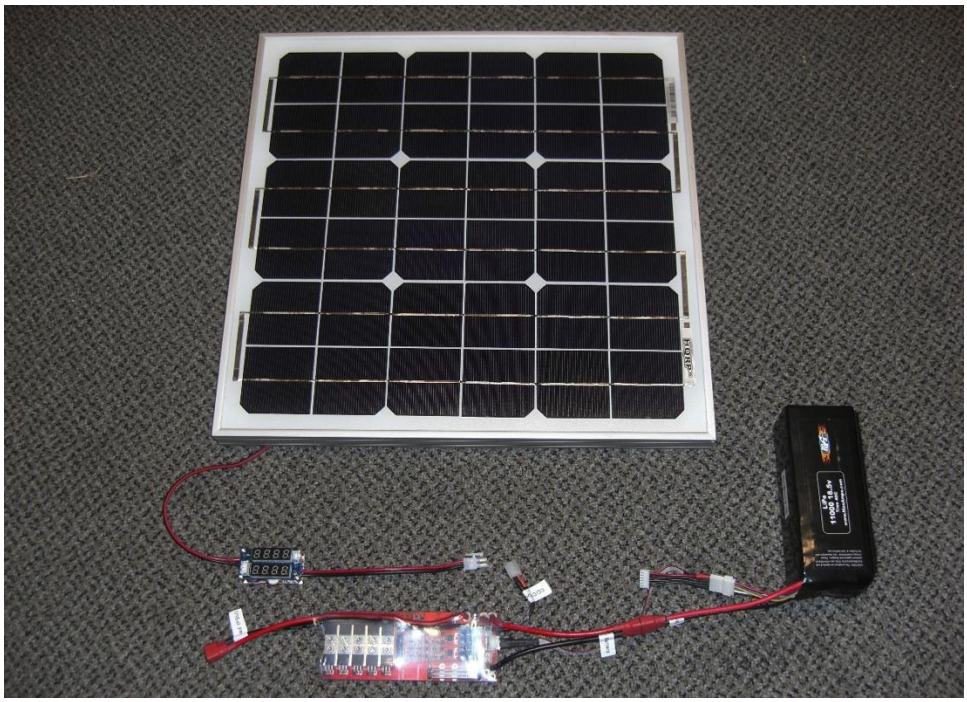

Fig. 27. Photograph of the current solar recharging system removed from the vehicle.

The current solar recharging system uses a commercially available 20 Watt monocrystalline silicon solar panel shown in Figure 27. This solar panel contains a total of 9 monocrystalline photovoltaic (PV) cells, and is used as a proof-of-concept to show that the solar recharging system is an effective way of recharging the batteries. Currently, a design is being implemented that covers the entire landing surface with a total of 24 PV cells for a total electrical output of 50 Watt under mid-day sunlight, as shown in Figure 28. The PV cells are critical to the effectiveness of the solar recharging system, because they are ultimately responsible for capturing the solar radiation and converting it into usable electrical energy. Equally important however, are the power electronics which allow the solar cells to actually charge the onboard batteries.

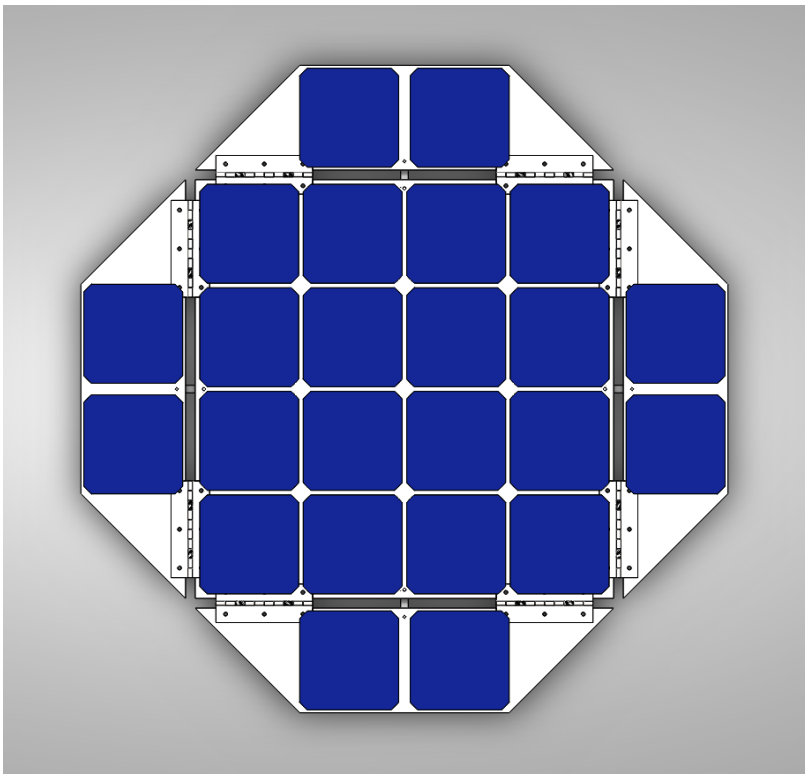

Fig. 28. PV cell layout on folding landing surface.

The power electronics which the solar recharging system implements are designed to be a generic as possible to allow for many possible PV cell configurations. This means that whether the system is using the 9-cell 20 Watt solar panel or the 24-cell 50 Watt solar array on the landing surface, the power electronics will charge the batteries and power the onboard systems either way. These electronics consist of two main components, a DC-DC boost converter and a battery management protection board, as shown in Figure 29.

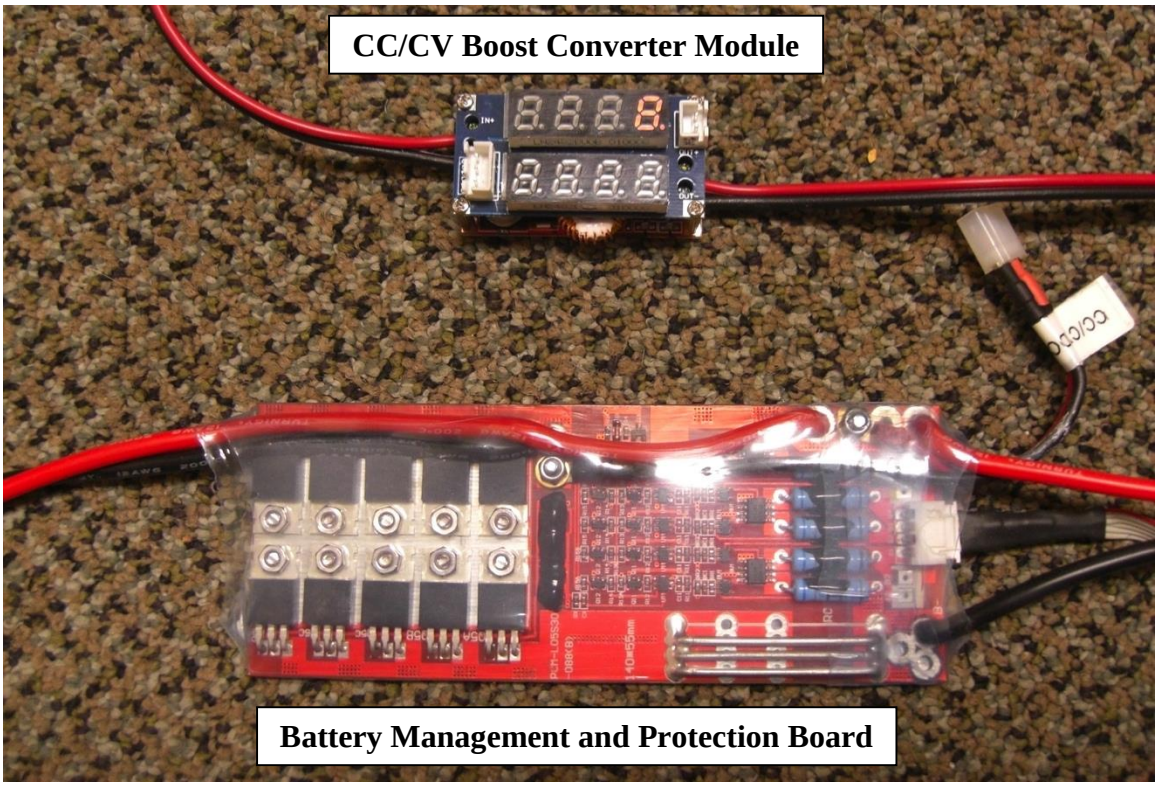

Fig. 29. DC-DC boost converter module & Battery management and protection board.

Charging lithium-polymer battery packs like the ones used by the landing platform is somewhat more involved than charging traditional Lead-Acid or Nickel Metal-Hydride

(Ni-MH) batteries. This is because lithium-polymer battery packs are more sensitive to improper charging and overvoltage. Lead-Acid and Ni-MH batteries have a higher internal resistance than lithium batteries, making them more forgiving to fluctuations in the charging voltage. If the charging voltage increases slightly for Lead-Acid or Ni-MH it will cause the charging current to also increase slightly, according to Ohm's law, because the internal resistance is relatively high. In a lithium battery however, a small increase in the charging voltage can lead to a large increase in the charging current; and if this happens unexpectedly, the battery can catch fire or explode. There are two important ways to help avoid these dangerous events, understand the proper method for charging lithium-polymer batteries and include protection circuitry that prevents the battery pack from accidental misuse.

When it comes to the correct method for charging lithium-polymer batteries, it is important to understand the difference between constant-current (CC) and constant-voltage (CV). A lithium-polymer battery must be charged using constant current while the battery is below a voltage of 4.20 Volts per cell. This means that the charging voltage is modulated so that the charging current remains constant at all times. The charging current depends on the batteries capacity, discharge rate and the manufacturer's recommendations. Generally speaking, the charging current should never exceed 1C (1 * the battery capacity), which in this case is 11 Amps per battery pack based on their 11 Amp-hour capacity. Once the battery pack reaches a voltage of 4.20 Volts per cell, the charger switches over to constant-voltage mode and maintain this voltage as the charging current is gradually decreased to zero. Once the charging voltage is 4.20 Volts per cell and the charging current is near zero, the battery is considered fully charged. All of the

CC/CV functions for the solar recharging system are handled by the boost converter module shown in Figure 29. This component takes the voltage from the PV cells, which is approximately 17 Volts, and steps it up to the proper level needed to charge the batteries correctly. The charging curves produced by the solar charging system on the landing platform are shown in Chapter 4 with the other experimental evaluations.

Another important consideration is whether the lithium-polymer battery contains two or more cells connected in series, in which case there must also be a method for balancing these cells so that they maintain an equal voltage. The landing platform battery packs each contain five cells connected in series (5S), so the solar recharging system also includes the cell balancing circuitry. This balancing circuitry tracks the voltage of the lowest cell and discharges the other four cells individually through metal film resistors until they are all equal. This task is handled by the battery management and protection board, as shown in Figure 29. This circuitry performs a number of other functions as well. It prevents the battery from being over-charged and over-discharged by disconnecting the battery pack if the voltage is not between 3.00 Volts and 4.35 Volts per cell. It also disconnects the battery if the charging current or discharge current exceeds 20 Amps for more than 3 seconds. All of these protection functions are handled using solid-state electronics, so there are no moving parts which are used to disconnect the battery from the landing platform systems. These protection circuits also feature automatic recovery that reconnects the battery pack as soon as the fault condition has been resolved. Each of the four battery packs is equipped with its own battery management and protection board. A schematic of the entire solar recharging system is shown in Figure 30. In this schematic,

the bypass diodes divert the current past any of the PV cells that are being shaded by the helicopter.

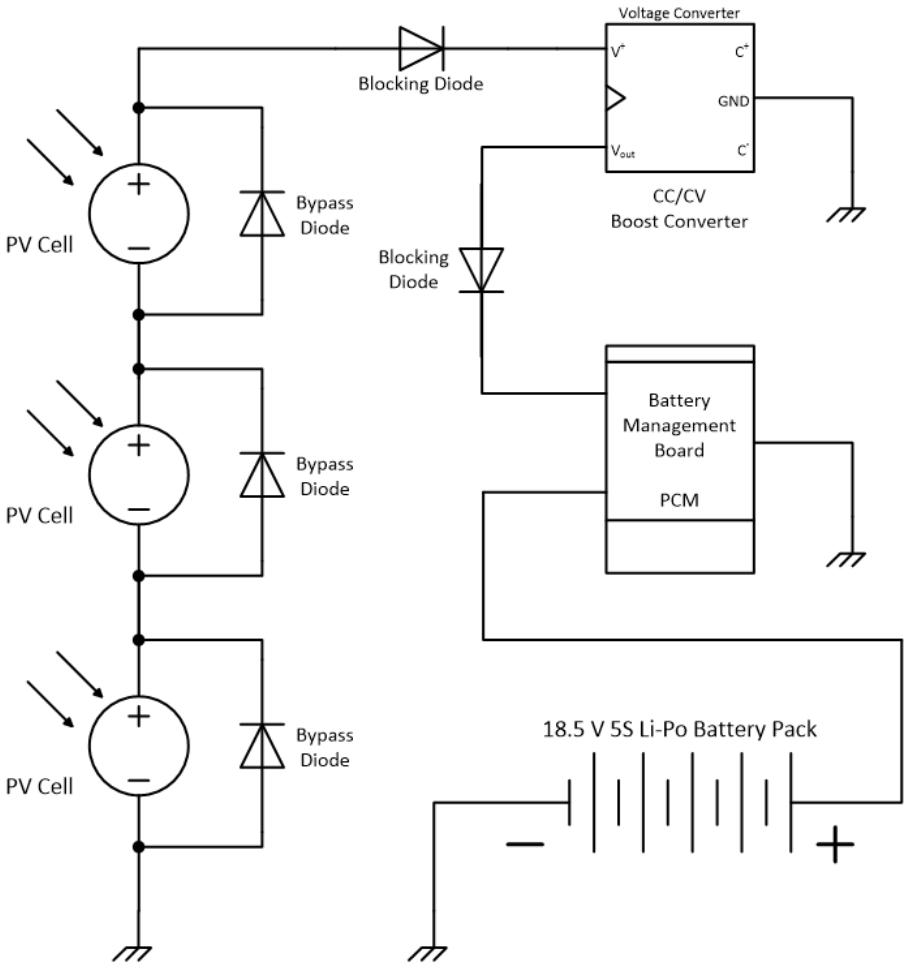

Fig. 30. Schematic of the solar recharging system.

Control, Communication and Sensors

Another section of the electrical design of the landing platform focuses on how the vehicle is controlled, how it interacts with a human operator and how it perceives its environment. At the center of the landing platform's control system is the XMOS XC-1A digital microcontroller shown in Figure 31. This piece of hardware is essentially the

“brain” of the vehicle, and is ultimately responsible for controlling all of the onboard systems. The XMOS XC-1A has a quad-core CPU that is capable of handling up to 32 simultaneous tasks with tight real-time scheduling. This distinctive capability allows it to monitor data from the sensors, control the wheel motors, operate the linear actuators, and communicate with human operators in parallel. XMOS technology is well-suited for controlling unmanned vehicles as discussed in [17]. The XMOS operates exclusively with a configurable 58-pin digital interface, meaning it has no ability to interpret raw analog signals. To handle the analog signals from the inclinometer and the actuator position feedback, the XMOS relies on two Linear Technologies LTC1865 dual-channel 16-bit Analog-to-Digital Converters (ADCs). Combined with a Texas Instruments TS3A5017 dual 4-1 multiplexer, the XMOS has the ability to interface with up to 10 different analog signals.

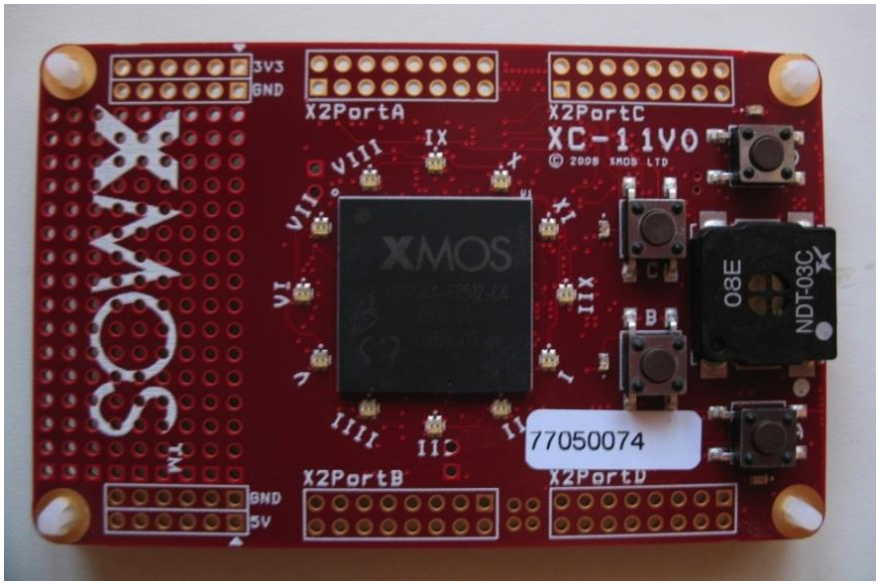

Fig. 31. XMOS XC-1A digital microcontroller.

Currently, communication between the human operator and the landing platform is accomplished wirelessly using a NXP Semiconductor WiFly module. This allows the operator to connect directly to the landing platform using any WiFi-enabled device, such as a laptop, tablet or smartphone. Once connected to the landing platform WiFly, the operator can send commands to the vehicle while at the same time receiving routine information regarding the status of the onboard systems. All of this data is handled by the XMOS. An external 2.4 GHz antenna is mounted to the outside of the vehicle on the rear body panel. This is necessary, because the aluminum structure of the landing platform acts as a Faraday cage, preventing the signals from reaching the WiFly's integrated antenna. The WiFly is a convenient way to interface with the landing platform, but its range is limited to approximately 50 meters. In the future, the landing platform will be equipped with a FreeWave 900 MHz radio system that has a range of more than 50 miles.

All of the electronics discussed so far in this section are mounted to a custom manufactured Printed Circuit Board (PCB) shown in Figures 32 and 33. The purpose of integrating all of these components into a single circuit board is to simplify the numerous electrical connections required to interface with the vehicle. As mentioned above, the XMOS XC-1A has a total of 58 digital I/O pins, and all but 6 of them are used to control the onboard systems. To wire all of these connections directly to the XMOS would be tedious and would make removal and replacement difficult. The PCB breaks out all of the I/O pins into groups so that each of the subsystems can be connected with a single locking connector. This keeps the control system organized and minimizes the possibility of damaging the XMOS. It allows for easy removal and replacement of any faulty component, as well as quick installation of all of the control electronics. The PBC control

board was designed using the CadSoft EAGLE software package, and custom manufactured by PCBcart.

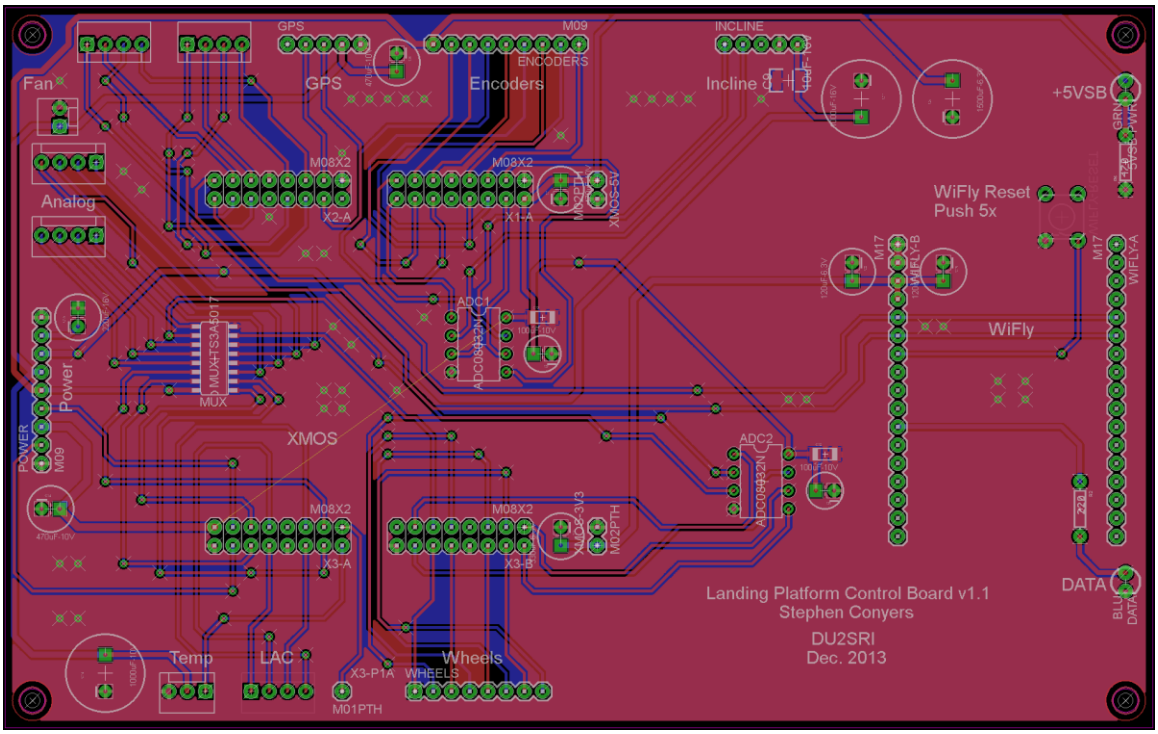

Fig. 32. EAGLE CAD design of the control board PCB.

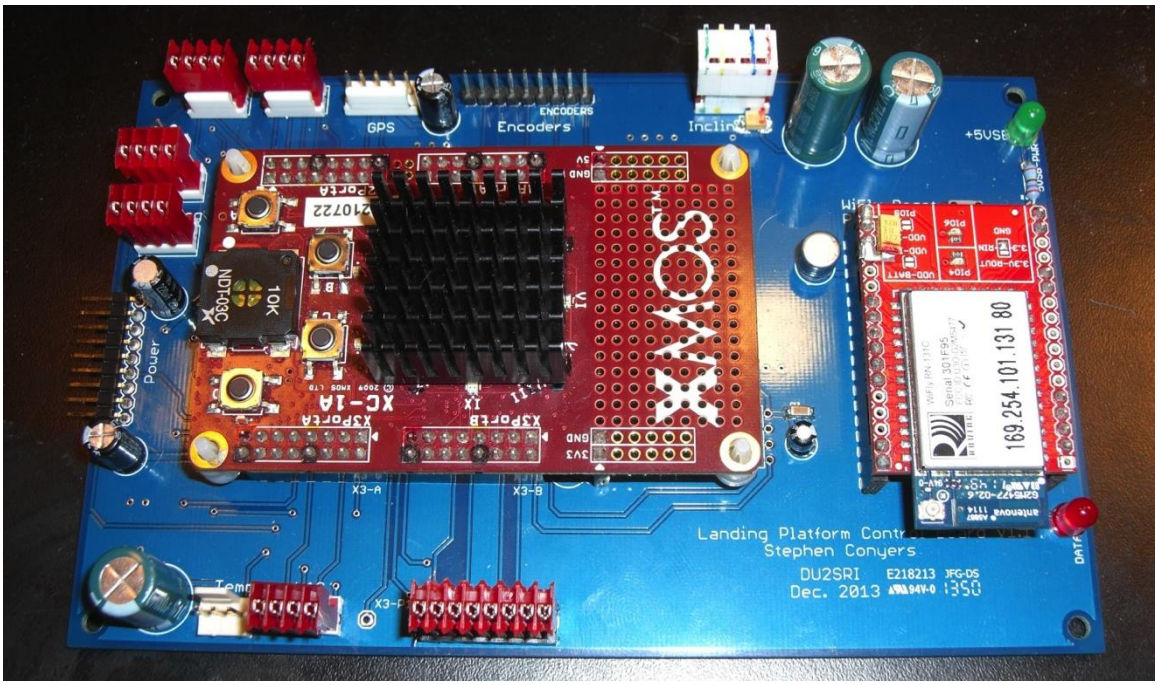

Fig. 33. PCB control board with the XMOS, WiFly, ADCs and Multiplexer.

The landing platform prototype has a number of sensors at its disposal that serve to increase the vehicle's self-awareness. To allow the vehicle to be semi-autonomous, it needs to be able to sense its environment and the current status of its onboard systems. The inclinometer and actuator position feedback are both described in Chapter 2, along with the wheel encoders. In addition to these sensors, the landing platform also includes a MediaTEK GPS unit and a digital temperature and humidity sensor. The GPS unit communicates with the XMOS through a Universal Asynchronous Receive and Transmit (UART) interface. This is a basic wired communication interface that uses two wires, a receive (RX) and a transmit (TX). Using the UART interface, the GPS sends regular updates to the XMOS that can include the latitude, longitude, elevation, speed, heading and more. This information can be filtered by the XMOS to only recognize what is

important for the vehicle's operation. The landing platform uses this information to determine its position and potentially navigate to a waypoint autonomously.

The digital temperature and humidity sensor is mounted inside the landing platform body, and is monitored by the XMOS to keep track of the conditions inside the vehicle. If the temperature increases above a predefined threshold, the XMOS can shut down the DC-DC converter and effectively put the vehicle to sleep until the internal temperature cools off. The ability to sense the relative humidity inside the vehicle is also a useful feature for determining if water condensation is building up inside the vehicle. Again, the XMOS can shut down the vehicle's other electrical systems if water damage becomes a possibility. The temperature and humidity sensor communicates with the XMOS over a one-wire interface. In this configuration, the XMOS sends a request to the sensor for the temperature and humidity information. The sensor then takes measurements and sends the data back to the XMOS over the same wire. This interface is simple from a hardware standpoint, but can lead to collisions when both devices are trying to send information at the same time.

There is an additional connection available on the control board for an ultrasonic distance sensor such as a Parallax PING sensor. This sensor could further aid in autonomous operation, allowing the landing platform to detect objects that are nearby (less than 3 meters). It is also possible that more sophisticated sensors such as laser scanners or stereoscopic cameras could be added to the landing platform in the future. These additions would further aid in autonomous operation, and allow the vehicle to navigate an environment without a human operator.

Software

All of the programming of the landing platform was done in using the XMOS-specific programming language known as XC. This language is a variation of regular C that has been specifically tailored to XMOS devices. It includes additional functionality that accommodates the unique capabilities of the XMOS architecture. Additionally, it still allows the user to use all of the normal C functions in a separate file if necessary, because not all of them are available in the XC language. More information about the unique features of the XC programming language can be found in [20].

The user interface between the landing platform and the host device uses a TCP/IP connection. This allows the operator to send commands and receive status updates from the vehicle using the same method that the operator might use to access the internet. This simplifies the connection between the user and the vehicle. The original user interface is a command line interface that uses single character commands to control the landing platform. Every quarter-second, the landing platform sends back a string of characters that communicate the status of the onboard systems to the operator. This interface takes some practice to be able to control the vehicle effectively. To shorten the learning curve and allow any user to quickly learn to operate the landing platform, a Graphical User Interface (GUI) was developed for the landing platform, as shown in Figure 34. The GUI was developed using Java, and allows the operator to just click a button and send a command to the landing platform. The vehicle's status updates are reported using sliding indicators, shown on the right side of the screen in Figure 33. This is a more intuitive way of understanding how the vehicle operates. The GUI is actually based on the same

character commands and status updates that are used in the command line interface, it just masks this interface with a user-friendly window.

Fig. 34. Graphical User Interface for the landing platform.

CHAPTER 4: EXPERIMENTAL EVALUATION

Self-Leveling System

Substantial field-testing has been performed on the landing platform prototype vehicle. The experimental test results are described in this section and compared to the original design requirements. The tests of the self-leveling system are described in this section, and consist of three separate experiments. The first set of tests are for the X-axis, which is the transverse direction from side to side. A photograph was taken of this experiment as it was being performed, and this is shown in Figure 35. The setup for the transverse X-axis test consists of placing the vehicle sideways on a slope of 24 degrees. Next, the auto leveling system was toggled ON and allowed to level the vehicle. The angle of the vehicle is monitored in real time over the command line interface every 250 milliseconds as it's reported by the inclinometer, and the data was recorded after each test was completed. The results of the three tests in this experiment are shown superimposed in Figure 36 as a plot of the landing surface angle as a function of time.

Fig. 35. Photograph of the transverse X-axis self-leveling test.

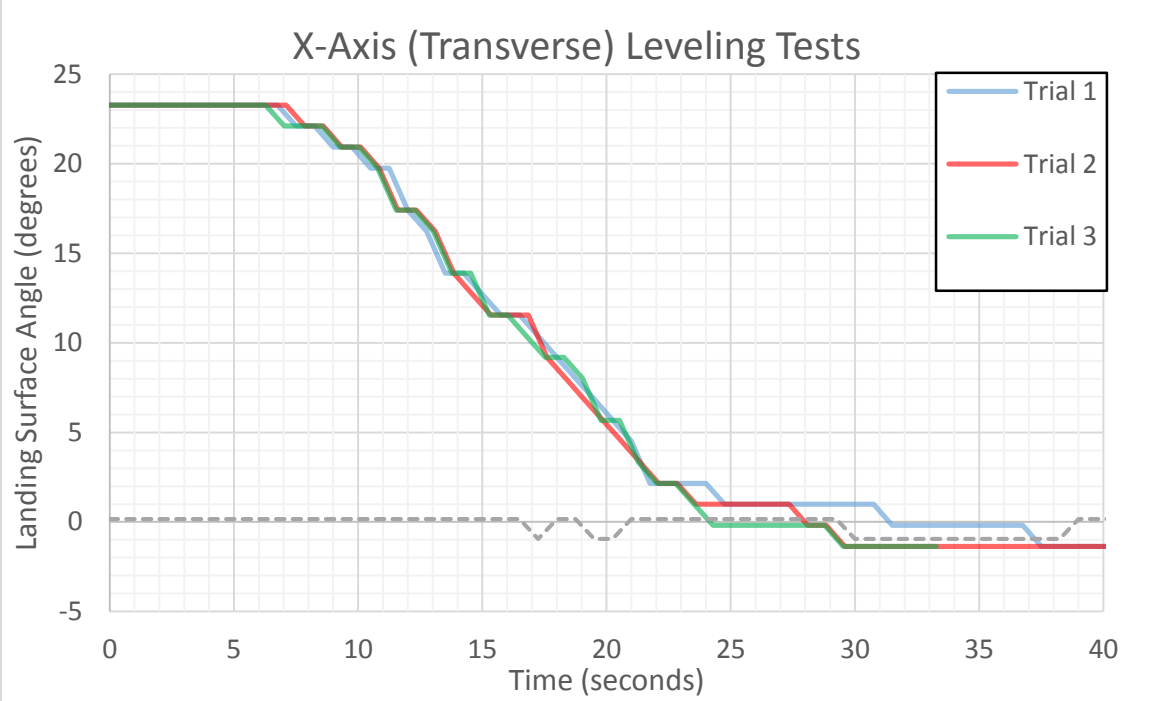

Fig. 36. Plot of vehicle angle as a function of time for transverse X-axis leveling.

The second set of tests are for the longitudinal Y-axis of the vehicle, which is the axis from the front to the rear of the landing platform. These tests follow the same procedure as the previous ones performed for the X-axis, and a photograph of this test is shown in Figure 37. This experiment uses the same 24 degree angle and also consists of three trials that are shown in Figure 38 as a plot of vehicle angle as a function of time. Additionally, before each of the three tests in this experiment, the landing platform was driven up onto the 24 degree slope and held there under its own power. It did not struggle to ascend this slope and did not slide back down. This serves to validate the requirement that the vehicle be able to climb a 28% grade.

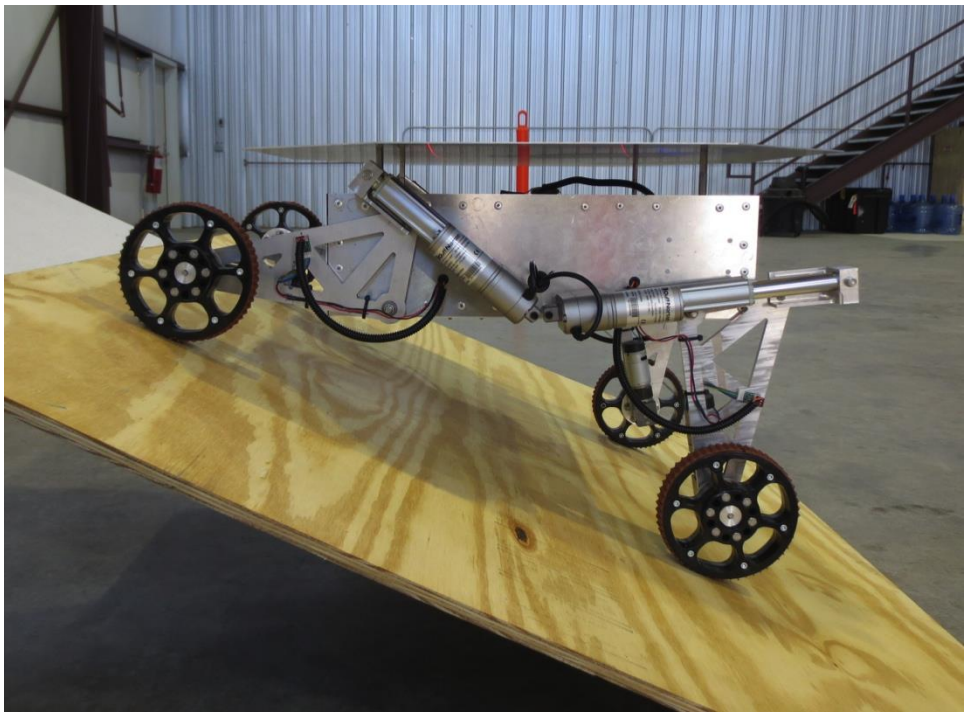

Fig. 37. Photograph of the longitudinal Y-axis self-leveling test.

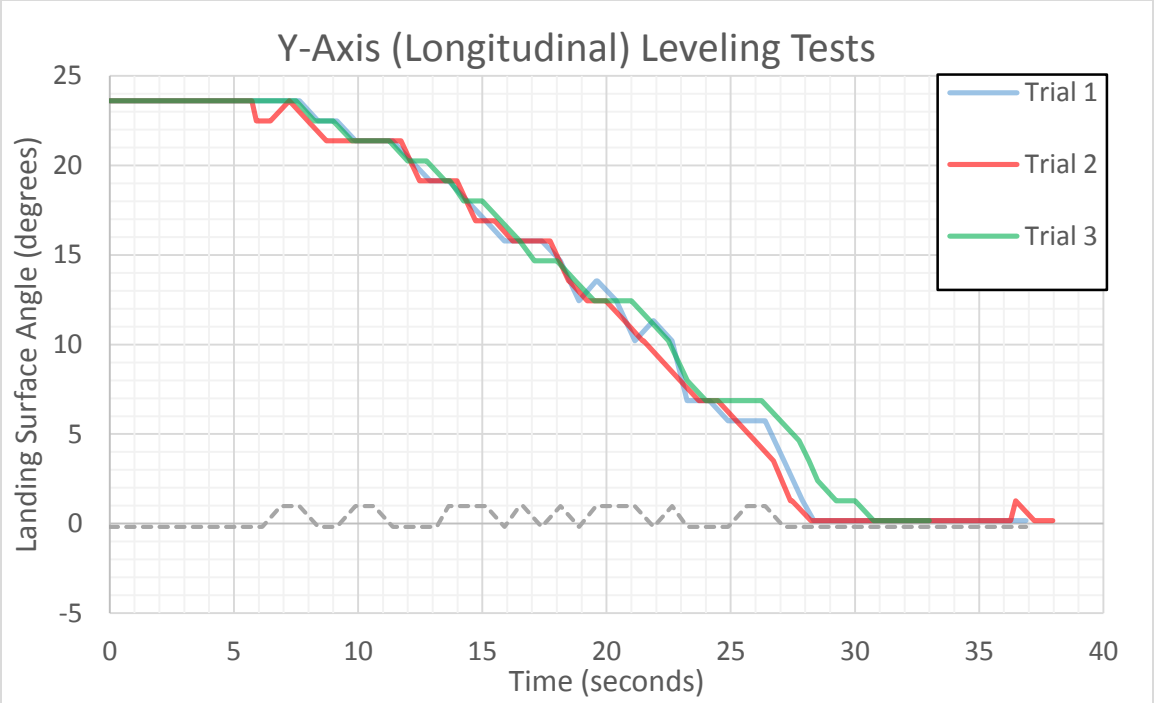

Fig. 38. Plot of vehicle angle as a function of time for longitudinal Y-axis leveling.

The final test of the self-leveling system combines the X- and Y-axis by placing the vehicle diagonally on a slope. This test serves to show that the landing platform can level itself regardless of the vehicle's orientation with respect to the slope. The angle of the slope in this experiment is 18 degrees, and a photograph taken during this test is shown in Figure 39. This experiment follows the same procedure as the previous two with the exception of the angle of the slope. The superimposed results of these three trials are superimposed in the plot shown in Figure 40. In all three of these experiments, the landing platform reaches a level orientation without any intervention from the operator within approximately 30 seconds. This data shows that the self-leveling system is an effective and efficient way of leveling the landing platform.

Fig. 39. Photograph of combined self-leveling test.

Fig. 40. Plot of vehicle angle as a function of time for combined leveling.

Drive System

The second series of experiments serve to evaluate the locomotion system of the landing platform. The primary design requirement for the locomotion system is that the vehicle must be able to reach speeds of 1.4 m/s (5.0 km/h). An indoor speed test is conducted in an aircraft hangar with a polished concrete floor, and consists of a series of six timed trials (three forward and three in reverse) along a 10 meter straight trajectory at full speed. The results from this test are averaged, and show that the vehicle takes an average of 6.98 seconds to cover the 10 meter, distance giving an average speed of 1.435 m/s (5.166 km/h). This test data shows that the landing platform meets the design requirement on a low-friction level surface.

Additional speed tests are conducted outdoors, the first of which involves timing the vehicle at full speed in both directions (forward and reverse) along a 100 meter straight trajectory over rough asphalt. The asphalt surface in this test is the tarmac at the Front Range Airport. The position data for the distance covered during the test comes from the onboard GPS module, and is recorded through the command line interface every 250 milliseconds. The vehicle takes an average of 77.52 seconds to cover the distance giving an average speed of 1.286 m/s. This result is somewhat lower than the indoor speed test because of the added friction from the rough asphalt surface. The tarmac is considerably more uneven than the hangar, and had numerous cracks and depressions.

A similar speed test is conducted over a similar distance on an uneven, muddy and partially snow-covered surface with tall grass and weeds. In this case, the test surface was the grassland fields between the taxiways at the Front Range Airport, and included a one meter deep drainage ditch as an added obstacle. The vehicle traversed this off-road terrain

with an average speed of 0.952 m/s. Again, the slower speed is due to the added resistance of moving across the off-road terrain. A velocity profile of the off-road speed test is shown in Figure 41 as a plot of velocity versus time. In the velocity profile it appears that the vehicle occasionally exceeds its maximum speed, but in fact this is caused by the GPS registering the change in position as a series of sudden jumps from one location to another. Because it cannot always be expect that the batteries will be fully charged during real-world operation, all of these drive system tests are performed with the batteries at 19.0 V, approximately 50% capacity.

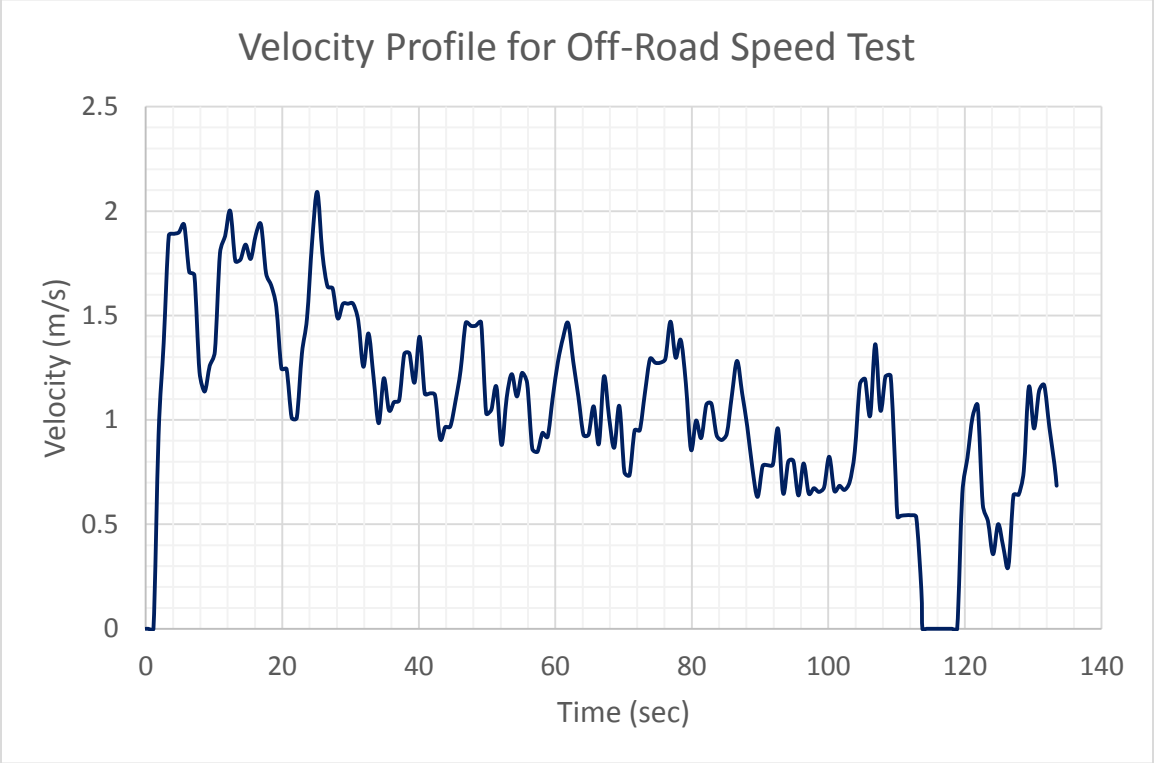

Fig. 41. Velocity profile of off-road speed test.

The final set of tests focus on the turning capability of the differential drive system by timing the completion of 10 rotations. Similar two the previous drive system tests, this experiment consists of 5 clockwise rotations and 5 counter-clockwise rotations, and the results are averaged. These tests are conducted with the vehicle in the most upright configuration with the shortest wheelbase length. This is the configuration in which the vehicle can turn most effectively. Again, three trials of 10 rotations are performed, and the vehicle takes an average of 5.43 seconds to complete a single rotation. This equates to an average angular velocity of 1.157 radians/sec (66.3 degrees/sec).

Solar Recharging System

The final experimental test serves to evaluate the solar recharging system. In this test, the 9-cell 20 Watt solar panel was placed 60 centimeters under a 1000 Watt High-Pressure Sodium (HPS) lamp. The reason for performing this test under a high-powered lamp instead of using sunlight is for consistency. The purpose of this test was not to evaluate whether the solar panel can produce an electric current, but rather to evaluate how well the power electronics charge the battery. To ensure a constant amount of power from the solar panel, a high-powered HPS lamp is used that closely replicates the power of the sun and the wavelengths of light used by the PV cells to produce electricity. The charge curves for current and voltage as a function of time are shown in Figures 42 and 43 respectively. These curves closely match the ideal charging for lithium-polymer batteries, and show that this is an effective charging system for the battery packs. The fluctuations towards the end of the charging cycle on the charge current curve are due to the balancing circuitry working to balance the cells. The balancing function only begins operating

towards the end of the charging cycle, and draws a small amount of current as it discharges any cells that are higher than the reference cell.

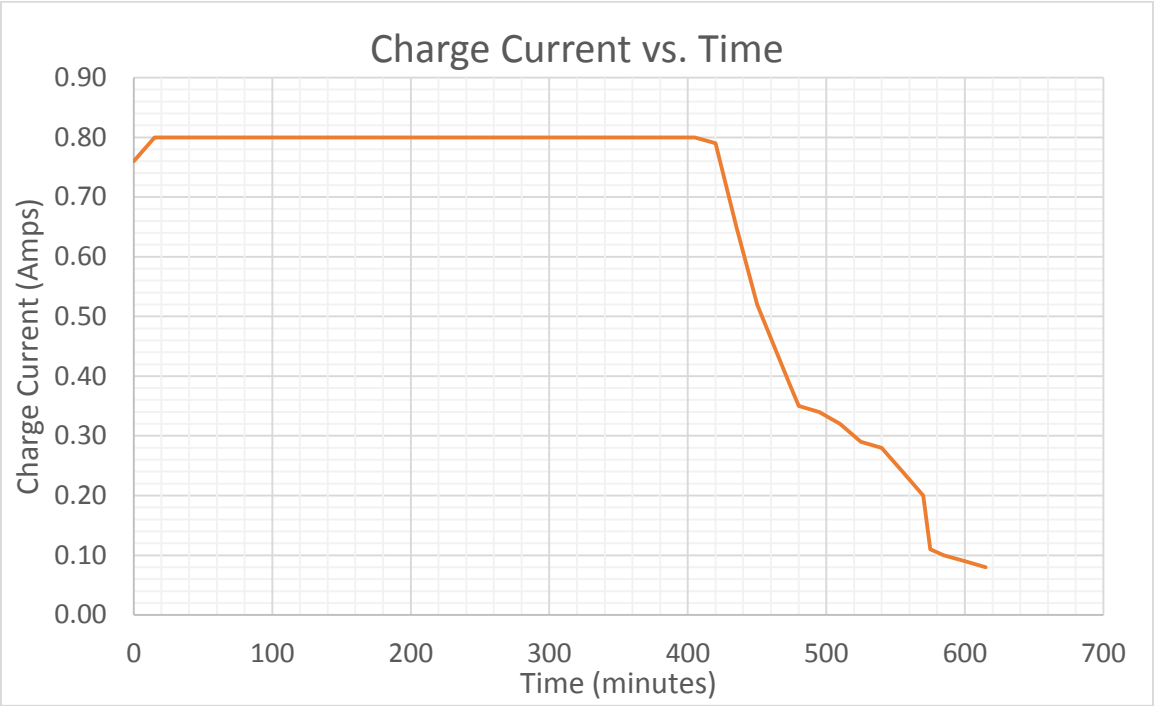

Fig. 42. Plot of charging current as a function of time.

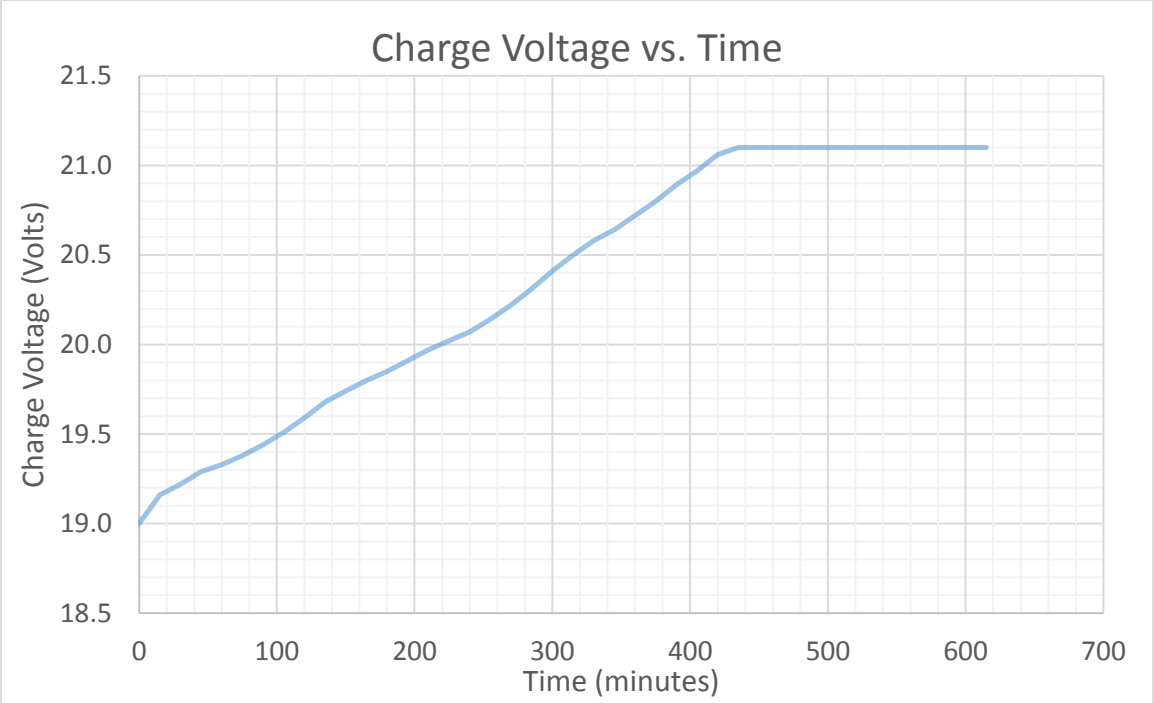

Fig. 43. Plot of charging voltage as a function of time.

CHAPTER 5: CONCLUSIONS AND FUTURE WORK

Future Work

Currently, the folding landing surface is still under construction. Most of the components have already been fabricated, but the system still needs to be installed on the vehicle and tested. Once the folding landing surface is installed, the custom photovoltaic cell arrangement will be installed on the landing surface. This solar collection array will greatly increase the output of the solar recharging system, and allow the landing platform to operate in the field indefinitely.

Another a system that allows the landing platform to recharge the helicopter after each flight is also being developed for the landing platform. The literature describes some methods that have been successfully implemented to swap the battery on a small UAV without human intervention [10-11]. These systems allow the vehicle to perform multiple flights without the limitations of traditional UAVs that need a human operator to change the battery after each flight. We would like to accomplish the same goal for vehicles using our landing platform as a base station in remote locations. Rather than swapping batteries, we propose to use a wireless inductive charging system to accomplish this goal. This system will consist of a 25 cm circular induction coil sitting on top of the landing surface. The UAV will be equipped with a similar coil on the landing gear. When the charge coil

on the landing platform is energized, it will wirelessly charge the UAV's battery. We plan to implement a prototype of this system in the near future.

Conclusion

This paper presents an intelligent, mobile, self-leveling landing platform for increasing the autonomy and endurance of small VTOL UAVs in the field. A prototype vehicle has been designed, built and tested, and this system is capable of navigating to a remote location, and remaining in an isolated area for extended periods of time without requiring any human intervention. It provides a level landing surface for autonomous unmanned helicopters and multi rotor aircraft, and serves as a base station for aerial vehicles in remote or inaccessible areas. An experimental evaluation of the self-leveling system, locomotion and turning capabilities and solar recharging system show the vehicle meets its design requirements.

REFERENCES

[1] K. D. Mullens, E. B. Pacis, S. B. Stancliff, A. B. Burmeister, T. A. Denewiler, M. H. Brunch, and H. R. Everett, "An automated UAV mission system," in *AUVSI Unmanned Systems in International Security 2003 (USIS 03)*, London, England, Sept. 2003.

[2] K. Mullens, A. Burmeister, M. Wills, N. Stroumtsos, T. Denewiler, J. Pachura, G. Prior, and B. Hawkins, "Automated launch, landing and refueling technologies for increased UGV-UAV effectiveness," in *1st Joint Emer. Prep. & Response/Robotic & Remote Sys. Top. Mtg.*, pp. 164-170, Feb. 2006.

[3] MDARS Vehicle Datasheet [Online]. Available: <www.jpeocbd.osd.mil/fps/Docs/Brochure%20for%20MDARS%20Aug2008.pdf>

[4] C. Cheung, B. Grocholsky, "UAV-UGV collaboration with a PackBot UGV and Raven SUAV for pursuit and tracking of a dynamic target", in Proc. SPIE 6962, Unmanned Systems Technology X, April 16, 2008.

[5] F. A. Chouery, "Stabilizing surface for flight deck or other uses," U.S. Patent 7040247 B2, May 9, 2006.

[6] R. Vogelaar. "Black Hawk Helicopter Crashed into a Navy Ship."Internet: http://www.aviationnews.eu/2009/10/23/black-hawk-helicopter-crashed-into-a-navy-ship/, Oct. 23, 2009 [Feb. 05, 2014].

[7] Los Angeles Times. "Marines Halt Search for Copter Lost at Sea."Internet:http://articles.latimes.com/1998/sep/19/news/mn-24411, Sept. 19, 1998 [Feb. 05, 2014].

[8] M. J. Zeno. "Design of an Autonomous Self Correcting Platform Using Open Source Hardware." MSME thesis, Rensselaer Polytechnic Institute, Hartford, CT, 2011.

[9] Y. Yu, J. Yi, C. Li, D. Zhao, and J. Zhang, "Control of a rope-driven self-leveling device for leveling adjustment," in *American Control Conference 2009*, pp. 5115-5120, June 2009.

[10] T. Toksoz, J. Redding, M. Michini, B. Michini, J. P. How, M. A. Vavrina, and J. Vian, "Automated battery swap and recharge to enable persistent UAV missions," in *Infotech@Aerospace*, March 2011.

[11] K. A. Swieringa, C. B. Hanson, J. R. Richardson, J. D. White, Z. Hasan, E. Qian, and A. Girard, "Autonomous battery swapping system for small-scale helicopters," in *2010 IEEE International Conference on Robotics and Automation (ICRA)*, pp. 3335-3340, May 2010.

[12] R. Godzdanker, M. J. Rutherford, and K. P. Valavanis, "ISLANDS: A self-leveling landing platform for autonomous miniature UAVs," in *2011 IEEE/ASME International Conference on Advanced Intelligent Mechatronics (AIM)*, pp. 170-175, July 2011.

[13] R. Godzdanker, M. J. Rutherford, and K. P. Valavanis, "Improving endurance of autonomous aerial vehicles through intelligent service-station placement," in *2012 IEEE International Conference on Robotics and Automation (ICRA)*, pp. 3179-3184, May 2012.

[14] K. Dalamagkidis, S. Ioannou, K. Valavanis, and E. Stefanakos, "A mobile landing platform for miniature vertical take-off and landing vehicles," in *14th Mediterranean Conference on Control and Automation, 2006. MED '06*, pp. 1-6, June 2006.

[15] B. M. Yamauchi, "PackBot: a versatile platform for military robotics", in *Proc. SPIE 5422, Unmanned Ground Vehicle Technology VI*, 228, Sept. 2004.

[16] “The modern warrior’s combat load,” U.S Army, Center for Army Lessons Learned Report.

[17] G. Martins, A. Moses, M. J. Rutherford, and K. P. Valavanis, "Enabling intelligent unmanned vehicles through XMOS Technology," *The Journal of Defense Modeling and Simulation: Applications, Methodology, Technology*, vol. 9, no 1, pp. 71-82, 2012.

[18] Murata SCA121T-D03 Product Datasheet [Online] Available: < http://www.muratamems.fi/sites/default/files/documents/sca121t_inclinometer_datasheet_82127400a2.pdf >.

[19] NASA Solar Radiation Data [Online] Available: < http://www.slideshare.net/solarengineer/solar-insolation-levels-in-north-america >.

[20] XMOS XC Programming Guide [Online] Available: < https://www.xmos.com/download/public/XMOS-Programming-Guide-(documentation)(B).pdf >.